RC beam models damaged and strengthened with GFRP strips under bending loading and free vibration

RC beam models damaged and strengthened with GFRP strips under bending loading and free vibration

by

R. Capozucca[1], E. Magagnini[2]

ABSTRACT

Four reinforced concrete (RC) beam models undamaged, damaged by notches and strengthened by external bonded (EB) glass fiber reinforced polymer (GFRP) strips have been experimentally studied. The paper aims to assess the availability of strengthening with EB GFRP strips in RC beams having a deep localized damage. The behavior of RC beams has been analysed under bending loading until failure. Furthermore, the assessment of RC beam models foresaw nondestructive control of damaged and strengthened models by free vibration tests to obtain frequency values at different damage degree. Damage, artificially obtained by notches with different width, on the midspan section and on the lateral location of beams, has been analyzed. The envelope of frequency response functions (FRFs) obtained by dynamic tests was elaborated and changes of natural frequency values are then correlated to damage both to non-strengthened beam with notches and to strengthened beam models. Results of static tests on RC beams strengthened with filled mortar in the notched sections and EB GFRP strips have allowed to validate the strengthening of RC elements with composite material characterized by relatively low elastic modulus; further, it has been assessed maintenance of bond between concrete surface and GFRP strips until failure under bending loading.

Keywords: RC beam models; damage; notch; GFRP-strip; vibration tests; bending tests.

[1] Professor of Struct. Engineering, Struct. Section DICEA, Università Politecnica delle Marche, Ancona, ITALY, phone +39.071.2204570 fax +39.071.2204532 r.capozucca@staff.univpm.it

[2] Post Doctoral PhD Eng., DICEA, Università Politecnica delle Marche, Ancona, ITALY e.magagnini@univpm.it

1. Introduction

The existing reinforced concrete (RC) structure of buildings and of high performance construction like bridges often present damages due to chemical processes of aggressive environmental conditions and, sometimes, they can be not be able to support new design service loads. In recent years, many repair methods have been proposed. A method of strengthening of damaged RC beams is the use of Fibre Reinforced Polymers (FRPs) and this technique was initially developed in Switzerland and Germany [1,2]. Strengthening with FRPs has been developed in recent years following two methods: FRP lamina or strips external bonded (EB) to the concrete surface of RC structures [3-7] or historic material [8] and FRP rods inserted into grooves of concrete covers utilizing the technique so called *near surface method* [9-12]. The two methods of strengthening have been experimentally investigated in many researches with interesting results [7,8,10]. Unfortunately, not all the aspects related to the behaviour of composite materials in the structural strengthening of RC elements have been completely solved, although many experimental and theoretical studies have been developed [12,14-16]. NSM as strengthening of RC beams appears capable to solve many aspects such as full FRP tension strength and to avoid damage deriving from impact and high temperature. This type of strengthening has been investigated by experimental tests and theoretical analysis also assessing the different factors affecting the bond of NSM FRP bars in concrete [12,17,18]. EB FRPs appears a technique more convenient when the damage is concentrated in limited zone as for damage due to local detachment of concrete for corrosion of reinforcement or for damage due to impact against the RC structures.

The deterioration of structure elements subjected to environmental chemical agents like pollution or to consequences of unforeseen state of local damage due to both impact loading and corrosion of steel reinforcement is coming an emerging duty of research in civil engineering. The aim of this work is both to acquire information on real structural elements through a laboratory experimental campaign on RC beams in scale and to underline a number of aspects that can be useful in practice

about the efficiency of strengthening with GFRP strips in RC beams in presence of local damage of the support.

In this paper an investigation is described regarding the use of GFRP strips to strengthen RC beams damaged by notches in any zone of span with different degree of damage linked to the width of notches. The choose to damage the RC beam models by notching derived from the purpose to investigate the effect of a localized damage with high reduction of global stiffness, such as local detachment of concrete.

In the experimental tests three beam models have been subjected to notches: one in the midspan section and two in one side and symmetrically respect the midspan section. After the strengthening with mortar filled in the notches and EB GFRP strips the beams were tested by bending loading until the failure. The results allow analysing the response of RC beams strengthened with GFRP strips.

The use of GFRP in the strengthening of RC beams is still an open field of research [18-21]. GFRP composite material is characterized by low Young's modulus and not relevant value of strength although the ultimate elastic strain under tensile stress is adequate in the practice. The availability of GFRP strengthening in RC beams is based on at least two important factors: the maintaining of bond between concrete and strengthening until failure of beam; the capacity of GFRP strips to improve the performance of damaged beams restoring the ultimate condition for RC beams under bending loading.

In this paper, the vibration response of RC beams has been adopted as additional non-destructive method to control the damage condition of beams already utilized in other works [22-23]. Vibration frequency data have been acquired by experimental dynamic tests assuming as boundary conditions free ends. The dynamic tests were carried out on RC beams with damages by notches and successively at different step of bending loading tests at every cycle of experimental loading.

The basic concept behind vibration monitoring is that dynamic characteristics are functions of structures' physical properties, therefore any change caused by damage results in change in

dynamic response [24-26]. Damage detection and health monitoring of structural elements are currently relevant topics in civil engineering. Many works have been proposed in literature about inverse structural health monitoring techniques based on vibration data able to give an accurate assessment of damage in terms of location and severity [27-31].

Static and frequency values of tested RC beam models have been analysed and discussed below; they allow to confirm availability of strengthening with GFRP strips in RC beams where the damage is localized in some sections although with high reduction of stiffness.

2. RC beam models and set-up for vibration tests

Experimental tests were carried out on four RC beam models: B0, A, B and C with the same geometric and mechanical characteristics. The dimensions of the beam sections were 80mm·120mm and measured 1100mm in length. The steel reinforcement used was 4 bars measuring 6mm and two in tension and two in compression and vertical stirrups at 50-100 mm intervals having a diameter of 6mm (Fig. 1(a) and (b)). The beams were characterized by concrete with Young's modulus E_c=28.43kN/mm^2 and steel bars with an average yielding tension equal to f_y=500 N/mm^2 [33,34].

Furthermore, the adopted steel reinforcement has been designed in order to obtain a scale model of real beam, which ensures the failure by bending and not by shear with a slenderness $h/l\approx$0.11.

One of the beam models B0 with same dimension and reinforced concrete was used as undamaged beam subjected only to bending test.

The experimental response of the three beam models A, B and C was analyzed both undamaged and damaged by notching on the concrete cover in different sections using dynamic tests considering free-free ends condition obtained by a suspension system (Fig. 2(a)). Successively, after the strengthening with external bonded (EB) GFRP strips was subjected to cyclic static bending tests and at each step of loading analysed again under free vibration tests.

The experimental dynamic test was carried out using a specific impact hammer through the well-known technique where a mobile accelerometer measures the acceleration of the structural element triggered with a hammer in a fixed point.

The accelerometer and the impact hammer (*Brüel & Kjær, Type 8202-2646*) have been connected to the data acquisition unit, respectively, on input channels. Before being able to proceed with the vibration tests, it was necessary to calibrate the data acquisition device in relation to the hammer, so as to obtain reliable results with minimized errors. A Fast Fourier Transformation (FFT) analyser, *Multichannel Data Acquisition Unit LAN-XI 3050 Type,* and PULSE Labshop software were used for the data acquisition in order to extract frequency values by transformed signals in frequency domain. In the dynamic tests the beam was subjected to impact load by hammer positioned in a fixed point at 50mm from the specimen's edge; the piezoelectric accelerometer was placed in succession on 5 positions named M_i with i= 1, ...,5 at different intervals (Fig. 2(b)). A set of 10 hits was made for each location of the accelerometer and the average value was acquired.

2.1. Vibration tests on beam models damaged and strengthened with GFRP strips

Undamaged RC beam model may be assumed for a first approximation, as a uniform slender beam neglecting gravity forces, the effects of rotary inertia, shear deformation and damping. For a beam in flexure only the component of displacement $v(x,t)$ may be considered. The inertia force of the element is $\rho \cdot A \cdot \frac{\partial^2 v}{\partial t^2}$ with ρ is density of the material and A is the cross-sectional area. In the case of natural vibration of a beam with homogeneous material, the well-known equation is obtained:

$$EI\frac{\partial^4 v}{\partial x^4} + \rho A\frac{\partial^2 v}{\partial t^2} = 0 \quad (1)$$

where: E is Young's modulus; I is the second moment of area of the cross-section; ρA is the mass per unit of length of beam. The solution of Eq. (1) allows obtaining the expression of circular natural frequency for generic r-mode of vibration in the case of both ends free:

$$\omega_r = \left(\alpha_r \cdot \frac{r\pi}{l}\right)^2 \sqrt{\frac{EI}{\rho A}} \quad (2)$$

being the eigenvalue $\lambda_r = r \cdot \pi / l$ for a simply supported beam. The eigenvalue for a free end beam at the *r* mode λ_r^f may be correlated to the value λ_r for a simply supported beam [32]: $\lambda_r^f = \alpha_r \cdot \lambda_r$ with a_r = coefficient that depends on the different *r* mode of vibration, equal to 1.506, 1.25, 1.167 and 1.125, respectively, for the first four modes.

By considering only the first four values of the eigenvalue λ_r^f and substituting the parameters of the experimental prototype shown in Table 1, the first four theoretical natural frequencies were calculated for the undamaged beam (Tab. 2). These frequencies were compared with the experimental frequencies recorded in the initial undamaged condition, D0. Table 2 contains a comparison between the frequency values theoretically evaluated considering a Euler–Bernoulli uniform beam for the first four (r=1, …, 4) modes, and the experimental frequency values obtained before artificial damage. The differences between the theoretical and experimental values are due to the theoretical stiffness value, EI, and density assumed for the theoretical analysis which are different respect to actual values, influenced by presence of reinforcement in concrete, variation of Young's modulus of concrete after 28 days from casting and experimental free-free end condition with elastic springs. In addition, a numerical modelling using Finite Element (FE) method has been carried out with the purpose to check the reliability of the experimental apparatus. The FE modelling has been performed with 3D ANSYS code. The beams' suspension system has been modelled by spring elements with a constant k equal to 0.01 N/m simulating the same free beam conditions in vibration. Modal analysis has been carried out to derive the first four natural frequencies of the beams and the natural frequency values obtained are contained in Tables 2. It is possible to notice that the theoretical results obtained with FE modelling are comparable with the ones given by experimentation. We can conclude that the suitability of experimental apparatus is confirmed.

As described above, the experimental vibration results were obtained through *frequency response functions* (FRFs), made up by complex matrixes, through which the parameters characterizing the dynamic behaviour of the structure were derived. Commonly, the form of the FRFs used in the

experimental technique is inertance, which returns a measure of the amplitude in terms of acceleration starting from random excitations through the Fast Fourier Transform (FFT) method. It is useful to consider a function referred to as coherence, which allows control over the results. Additionally, it is worthwhile checking that the value of the coherence is near one in order to evaluate the reliability of the measurements. The experimental program established that the data file regarding the frequency response would be re-elaborated, in order to evaluate the validity of the data obtained, for each of the measurements. Hence, it was decided that the data relative to the FRFs obtained from the experimentation would be presented in the FRFs' complex modulus vs. frequency form. The FRF envelopes, for every marks M_i with i=1, …, 5 are shown in Figure 3 for the undamaged condition.

The analysis of experimental vibration on damaged RC beams was lead taking into account three specimens having the same dimensions and mechanical characteristics as the undamaged RC beam. Damage has been obtained removing cover concrete at different position along the beam's length considering three types: model with damage due to one notch in the middle section of beam - type A; model with damage due to one notch on concrete cover in a lateral section at 200mm to the middle of beam – type B; and model with damage due to two notches symmetrically located on the beam two symmetric sections at 100mm from the midspan – type C (Fig. 4(a)). Further, the three RC beam models, with damage type A, B, and C, are studied with different degree of damages due width of notch (Fig. 4(a)). Experimental RC beam A was damaged by notches all over the middle section with three damage step D1-D2 and D3 at midspan section: for D1 the width of notch was equal 5mm; for the damage D2 the width of notch was equal to 10mm and for damage D3 the width of notch was equal to 15mm (Fig. 4(b)).

The experimental vibration tests of damaged beam models were carried out considering set-up of free-free ends (Fig. 4(a)) with the same impact technique described above. Natural frequency values measured at each width of notch as damage degree D1, D2, D3, are shown in the Table 3 for model

with damage type A; in the Table 3 the frequency variations in percent, $\frac{\Delta f_r}{f_{r,exp}^{D0}} = 100\frac{f_{r,exp}^{D0} - f_{r,exp}^{Di}}{f_{r,exp}^{D0}}$, are shown being experimental value $f_{r,exp}^{D0}$ the frequency obtained in undamaged condition D0.

The experimental FRF envelopes at the different damage degree with measures of vibration recorded by the accelerometer in a number of selected mark points, M_i with i = 1,…,4, for beam type A are contained in Figure 5. It is possible to observe the shift of the diagrams at various steps Di with reduction of the frequency values due to increasing of width's notch.

In a second phase, the notches were filled with thixotropic mortar (*Mapegrout by Mapei Company*) according to the configuration outlined as R1 and the vibration tests that result in the frequency values were repeated. Then, beam type A was strengthened with external bonded EB GFRP strips glued on the intrados and extrados of concrete surface for a length of 300 mm with width of 50 mm, as shown in Figure 6 and, finally, this configuration was labelled as R2.

An epoxy resin (*FLK* by *AhRCOS Company*) was adopted as the matrix and it is characterized by the following mechanical properties: Young's modulus E_{res}=1600 N/mm^2 and Poisson's modulus v_{res}≈0.48, obtained by compression tests on two prismatic specimens. The EB GFRP strip presents thickness t_{GFRP}=1.20 mm, tensile strength f_{GFRP}=1317 N/mm^2 and Young's modulus E_{GFRP}=64 GPa; they were obtained using tensile tests on specimens according to the ASTM-D 3039 Standard [35].

The vibration tests were performed also for this configuration. The experimental data recorded during the vibrational tests for these configurations were elaborated in frequency domain as already mentioned and shown in Table 3.

Figure 7 contains for beam model with notch type A, the comparison of the values of the variations, in percent for the experimental frequency as damage proceeds, for the four vibration modes r = 1,…, 4, relative to undamaged condition D0. It can be noted that, as expected, increase in damage reduces frequency values for the first modes of vibration with variation values equal to 35%÷45% for mode r=1.

The filling of the notch with thixotropic mortar and the application of the EB GFRP strengthening, configuration R2, act going to restore the continuity of the beam. This aspect can be seen through the experimentally recorded vibration response of the strengthened beam. In the case of damage degree R2, it is possible to observe an increase of the experimental recorded frequency with values close to those found in the undamaged configuration for r=2 and r=4 modes and with limited variations in frequency than not exceed 11% at the first mode r=1.

* * *

Second experimental RC beam model was damaged again removing concrete cover - damage type B - all over a section located along the axis of the notches at 200mm from the midspan section of beam with three damages or notch steps D1, D2 and D3 (Fig. 4(b)). In Figure 8 details of damage by notch in RC beam are shown. Free vibration tests were performed for each damage degree and the envelope diagrams of the FRFs extracted by the measurement apparatus described above, are compared for each step of damage from degree D0 to D3 are shown in Figure 9.

In a second phase, the notch was filled with thixotropic mortar according to the configuration outlined as R1 (Fig. 10(a)) and then the beam was strengthened with EB GFRP strip placed at the intradoss for the entire length of beam model with width of 50 mm - configuration R2 (Fig. 10(b)). The vibration tests that result in the frequency values were repeated for both the configurations. Table 4 shows the average frequency recorded experimentally for each step of damage degree from D0 to R2. The comparison of the values of the variations in percentage for frequency is shown in Figure 11. It can be noted that the expected trend is confirmed. In fact, until damage degree D3, the frequencies decrease with the increase of the notch's width with a maximum value equal to approximately 39% for the first mode r=1 and, approximately 28% for the second mode r=2. Once the damage has been repaired (configuration R1), a slight increase of the frequencies was recorded with a consequent decrease of the percentage variations. During the subsequent step (configuration R2), with the EB GFRP strengthening, it is possible to observe a wide increase of the experimental

recorded frequency with values close to those found in the undamaged configuration for r=2 and r=4 and with limited variations in frequency than not exceed 12% for the first mode r=1.

* * *

Third experimental RC beam model as indicated above was subjected to a damage named type C by notch all over two symmetric sections, placed at 100mm from the midspan, with three damage step D1-D2 and D3 increasing the width of notch in the same way, respectively, 5mm, 10mm and 15mm.

Natural frequency values were measured at each step of damage (Fig. 12) and the dynamic responses were obtained using, once again, the same methodology described above with impact by hammer and an accelerometer at four measurement points connected to an acquisition system working in a range of frequencies between 0 and 2500 Hz. The average experimental frequency values recorded at damage degrees Di with i = 0,...,3 are indicated in Table 5 with the variation of frequency in percent in relation to the different damage degree. The experimental FRF envelope diagrams recorded during vibration tests for damage degrees Di are shown in Figure 13. It is possible to observe a progressive reduction of the frequency values due to increasing of width's notch. Referring to the frequency variations values contained in Table 5, it can be noted that the variation is consistent also for a low level of damage as D1, with a value equal to approximately 43% for the first mode r=1 and, approximately 27% for the second mode r=2. The peak value is recorded at final damage degree D3, with a value equal to approximately 47% for the first mode r=1 and, approximately 32% for the second mode r=2. The notches were subsequently filled with thixotropic mortar according to the configuration outlined as R1 and then the beam was strengthened with EB GFRP strip placed at the intradoss for a length equal to 900mm and width equal about 50mm (configuration R2), as shown in Figure 14.

The experimental data recorded during the vibrational tests for both configurations were elaborated in frequency domain as already described. Table 5 contains the experimental frequency data recorded for the strengthened beams (R1 and R2) as well as the levels of damage due to notching.

Figure 15 contains the comparison of the values of the variations in percentage for the experimental frequency as damage proceeds, for the four vibration modes r = 1,…,4, relative to undamaged condition D0. It can be noted that, only by filling the notches with thixotropic mortar (configuration R1), it is possible to observe a wide increase of the experimental recorded frequency with limited variations in frequency that not exceed 3.6% in relation to D0 condition. The presence of the EB GFRP strip (configuration R2) acts by reducing more the frequency variations; it is possible to observe a further increase of the experimental recorded frequency with values very close to those found in the undamaged configuration and with limited variations in frequency equal to approximately 1.14% for the first mode r=1 and, approximately 1.3% for the second mode r=2.

3. Strengthened RC beam models under bending tests

Static tests were carried out on beams damaged and strengthened with EB GFRP strips and with notches filled using thixotropic mortar, by bending loading path increasing the load P applied at two points, 300 mm from the middle of the beam. In addition, a fourth specimen B0 was used as a reference and it was tested without damage due to notch and strengthening. Static tests were performed in order to verify availability of strengthening in tensile and compressive zone and to monitor possible local mechanism of delamination. The tests' set-up is shown in Figure 16(a). The beams were tested in hinge-hinge end condition by a specific steel support system. Particular attention was paid during the design and execution of the hinge condition. The beam was bound to the metal devise using 3+3 bolts, the contact was adjusted using a 3 mm metal disk and a 3 mm thick neoprene lamina. The instruments used in the static tests were a vertical jack to transmit the load P with a load cell to measure P and two strain gauges (E1 and E2) to record deformation during bending tests, one on the intradoss and one on the extradoss of beams (Fig. 16(b)). For beam with damage type A, in addition to the instruments described above, two horizontal linear transducers (LVDTs 1 and 2) to record deformation on each lateral surface of compressed concrete (Fig. 16(b)). All the beams were subjected to cyclic increasing load P1=3.0kN, P2=8.0 kN,

P3=12.0kN and at every load step were subjected to dynamic tests. After these cycles of loading the beams were subjected to increasing load until failure. Main results obtained during the static bending tests are summarized in Tables 6-9 where damage degree by bending test is shown as D*i with i=1,2,3 and it's linked to the value of bending load Pi reached at each one of the three cycle of bending loading.

The collapse of beam B0 happened at load value equal to P=15.77kN reaching the maximum experimental measured value of compressed concrete strain equal to $\varepsilon_c \cong 2.77 \cdot 10^{-3}$; the failure was due to crash of compressive edge of concrete and extensive cracking of the concrete in the tensile surface (Fig. 17(a) and (b)). The envelope of experimental diagram moment, M, versus curvature, χ, is contained in Figure 31.

Fig. 18 shows the development of cracking damage in strengthened beam type A. Detailed damage of EB GFRP strip is also shown in Fig. 18 where we can also witness the beginning of delamination buckling which occurred during damage state D*3 at the top of the beam's mid- span zone. The collapse, reached at a load value equal to P=14.89kN, happened with the complete detachment of GFRP strip for delamination buckling at the extrados and successively expulsion of the concrete cover at the intrados with detachment of the GFRP strip. An aspect that needs to be underlined is the high concentration of damage along the filled notch with the formation of local cracking mechanisms that may have cause the brittle failure of the entire system. From the measurements recorded in terms of strains at midspan of beam type A, the experimental diagrams shown in Figures 19(a) and (b) have been obtained. After the damage degree D*3, the strain gauge E1, positioned on the GFRP strip at the extrados of the beam, was no longer able to provide measurements due to the start of the delamination buckling process (Fig. 19(a)). Therefore, strains of the compressed edge were detected with two extensometers placed on the lateral faces of the beam. The envelope of experimental diagram moment, M, versus curvature, χ, evaluated considering the strains on compressed edge of midspan section and on intrados GFRP strip, is shown in Figure 31.

The failure of beams type B occurred at load value equal to P≈18.35kN caused by the crashing of the compressive edge of concrete and the GFRP rupture, with high concentration of damage at the filled notch (Fig. 20). In Figure 21, the strain values measured on compressive concrete, ε_c, on the GFRP strip, ε_{GFRP}, are shown for the all damage degrees. It is noted that the maximum value of strain recorded on the GFRP strengthening reached high value of deformation equal to about $8 \cdot 10^{-3}$. In Figure 31 the envelope of experimental diagram moment, *M*, versus curvature, χ, relative to the cross-sectional area, is shown with reference to the values measured on the compressed edge of midspan section and on GFRP strip.

For what concern beam type C, the collapse was reached at load value equal to P≈20.35 kN due to expulsion of the concrete cover at the intrados with the detachment of the GFRP strip. The typical cracking states at damage D*1, D*2 and D*3 together with failure state for beam type C are shown in Figure 22. Experimental diagrams load, P, versus strain at the edge of compressed concrete, ε_c, and strain at the tensile GFRP strip, ε_{GFRP}, are shown in Figure 23. Finally, the envelope of experimental diagram moment, M, versus curvature, χ, obtained for the cross section at the beams' mid length is shown in Figure 31.

4. Results of vibration tests at different steps of bending loading tests

Natural frequency values were measured at each step of bending loading. The dynamic responses were obtained using, once again, the same methodology described above with impact by hammer and an accelerometer at 5 measurement points connected to an acquisition system between 0 and 2500 Hz. The signals were recorded and elaborated in frequency domain through the FFT technique and FRFs obtained using Pulse software.

Average frequency values recorded experimentally for RC beam B0, without strengthening, at the various damage steps Di at each of the accelerometer positions are contained in Table 10 together with the frequency variations, in percent, $\frac{\Delta f_r}{f_{r,exp}^{D0}} = 100 \frac{f_{r,exp}^{D0} - f_{r,exp}^{Di*}}{D0}$. Figure 24 gives a comparison of the

experimental frequency values as damage proceeds, for the four vibration modes r=1, ..., 4, relative to condition D0 for beam type B0.

The main experimental frequency values data obtained from the analysis of free vibration for GFRP strengthened beams type A, B and C at the various damage steps Di are contained in Tables 11-13.

Average frequency values were recorded experimentally at each of the accelerometer positions and the frequency variations, in percent, $\frac{\Delta f_r}{f_{r,exp}^{R2}} = 100\frac{f_{r,exp}^{R2} - f_{r,exp}^{Di*}}{f_{r,exp}^{R2}}$, with reference to the different damage degree are also shown in Tables 11-13.

The experimental FRF envelopes, for the different damage degree, for every position point of the accelerometer, *Mi* i=1,...,5,, for strengthened beam type A, are shown in Figure 25. It is possible to observe the shift of the diagrams at various steps Di with reduction of the frequency values due to increasing of concrete cracking damage. Figure 26 contains a comparison of the experimental frequency values as damage proceeds, for the four vibration modes r=1, ..., 4, relative to condition R2 for beam type A.

The experimental FRF envelopes at different damage state Di i=1,…,3 with measures of vibration recorded by the accelerometer in a number of selected mark points, *Mi* i=1,...,5, for strengthened beam type B are contained in Figure 27, where it is possible to again observe the reduction of the frequency values due to increasing concrete cracking damage with the shift of the diagrams at various steps Di. The comparison of the experimental frequency values, as damage proceeds, for the four vibration modes, relative to condition R2 for strengthened beam type B, is contained in Figure 28.

Finally, the experimental FRF envelopes, for the different damage degree, at each point of the accelerometer, are shown for strengthened beam type C in Figure 29, where it is, once again, confirmed the shift of the diagrams at various steps Di with the increase of concrete cracking. Figure 30 contains a comparison of the experimental frequency values, as damage proceeds, for the four vibration modes, relative to condition R2 for strengthened beam type C.

5. Discussion of results

Static and dynamic experimentations allow the definition of a number of aspects that can be useful in terms of techniques used to strengthen RC beams with EB GFRP.

The first result that needs to be stressed is the behaviour of RC beams in relation to the different configuration of the strengthening system. From the result's analysis of experimental campaign performed on RC elements strengthened with EB GFRP strips placed at the tensile extrados, it can be noticed how the strengthening by EB GFRP equipped beams led to an increase in the moment capacity of reinforced concrete flexural members, equal to 16% and 29%, respectively, for beam type B and C in relation to B0 capacity. For beam type A, the increase in resistance is absent, due mainly to the mechanism of damage of the GFRP strip at the extrados that may be considered as combination of delamination buckling of compressive GFRP at extrados and presence of notch strengthened with mortar at mid span section.

The results obtained by experimental tests, allow observing that the strengthening of RC beams with EB GFRP strips on the tensile side is an efficient way to increase the strength of damaged beams. In particular, the GFRP strengthening conferred to the RC beams, above all, a greater capacity to increase strain under tension until the failure by compression of concrete, which is the conventional ultimate condition for RC beams under bending. Instead, in a system such as RC beam strengthened with GFRP strips on the tensile side and on the compressive side, the low Young's modulus of GFRP composite material and the formation of local cracking mechanisms can cause the debonding and subsequent local buckling of the FRP layer that can result in a premature failure of the strengthened RC beam. From the analysis of the behaviour of the GFRP strip under compression it is possible to state that the presence of the strengthening on the compressive side allows having an extradoxal reinforcement, which still works but is conditioned by the delamination buckling. After the beginning of the debonding of the GFRP strip, there is an increase equal to about 25% of the moment that the beam can withstand before failure (Fig. 31).

What is mainly observed in all cases investigated is that the strengthening conferred to the RC beams, above all, a good level of ductility under bending, with values of ductility ratio deduced by the ratio of ultimate curvature value, χ_u, on yield curvature, χ_y, greater that $\chi_u/\chi_y > 1.5$, for all cases investigated (Fig. 31).

The vibration analysis as non-destructive method of control of RC unstrengthened and strengthened is convenient. The results' analysis of the non-destructive dynamic tests gives important elements to the assessment of reliability of RC beams strengthened by EB GFRP under different load conditions and during the life of the beams. Considering the dynamic response of tested beams it can be noted that, in general, increase in damage reduces frequency values for the all first four modes of vibration r= 1,…,4.

A comparison between the dynamic experimental frequencies of the different beams highlights that damage is represented mainly by the cracking of the concrete. In fact, an increasingly relevant reduction of the frequencies recorded is had for increasing damage state, for all the strengthened beams subjected to vibration at different damage degrees. The cracking of the concrete influences the beams' dynamic response in both the non-strengthened and the strengthened condition reducing the values of the experimental frequency. Referring to the frequency variations diagrams contained in Figure 24, 26, 28 and 30, respectively for beam models B0, A, B and C, it can be noted that, the highest variation of frequency occurs at damage degree D1, when the first cracks appear, with values equal to approximately 16%-35% for the first mode r=1 and, approximately 15%-41% for the second mode r=2. The response of unstrengthened beam B0 under vibration allows us to verify a progressive and regular reduction of the variation of the frequency values with an increase in damage degree (Fig. 24) with a maximum value equal to approximately 65% for damage degree D3* for the first mode=1. Instead, the comparison of frequency variations for the response of the GFRP strengthened beams shows that, after damage degree D1, the variations between the different damage steps tends to be smaller and no longer constant. In fact, GFRP strengthening contributes to reducing the width of the cracks undergoing even heavy loads. For beam type A, the damage

condition represented by the cracking of the concrete and the local buckling of the GFRP layer, which occurred during damage degree D*3, results in the change of dynamic response of beam. In this case, it is possible to observe an increase of the frequency variation values (Fig. 26), in relation to the previous damage degree D*2, with a peak value equal to approximately 39% for the first mode r=1 and, approximately 44% for the second mode r=2.

An aspect that needs to be underlined is the evaluation of the influence of the local damage in the structural response of the system. The damage by notch represents a very strong and deep weakening in a zone where the maximum moment acts. The recovery of this local damage with thixotropic mortar and GFRP strip leads to an improvement of the general behaviour of the experimentally recorded frequencies that reach, after the strengthening, values approximately equal to the undamaged condition. This behavior under free vibration is due to refurbishment of the mass/density of beam. From the point of view of stiffness, however, the damage by deep notch leads to a substantial loss of stiffness, which is not recovered by the consolidation. In this case, the strengthening by EB GFRP allows an increase of the deformation capacity under loading although the stiffness of beam is on the whole smaller as it is possible to verify by the diagrams moment versus curvature for the tested beam models in Figure 31. From Figure 31, it can be noted how the presence of notch determines an important contribution in terms of stiffness' decrease in the strengthened RC beams subjected to static bending test. This aspect is particularly evident in the case of notch positioned at the midspan (beam type A) where a significant drop in stiffness has been recorded from EI=237 kNm^2 to 25 kNm^2 (in percent 68%); while turns out to be less important in the case of symmetrical double damage in the beam type C from EI= 237kNm^2 to 62.5 kNm^2 (in percent 49%). For beam type B, the presence of lateral damage by notch affects the behaviour of the model in terms of stiffness' reduction from EI= 237kNm^2 to 100 kNm^2 (in percent 35%).

Below, the variation in stiffness that the RC beam models undergo once subjected to static bending tests is developed from the analysis of frequency variations. The frequency variations for a beam model, for the four vibration modes r=1, ..., 4, may be expressed as follows:

$$\Delta f_r|_{Hz} = 100(f_r^{D0} - f_r^{D3})/f_r^{D0} \quad (3)$$

where f_r^{D0} and f_r^{D3} are the experimental frequency values obtained for beam specimens, respectively, for undamaged condition D0 and for damage degree D3 by notch damage.

The natural frequencies for the beam models may be theoretically evaluated by the following expression:

$$f_r = \lambda^2 \left[\frac{EI}{\rho A}\right]^{0.5} \quad (4)$$

where: λ = the eigenvalue; ρA = the density for unit of length and EI = the bending stiffness. Introducing the Eq. (3) into Eq. (4) the following expression can be obtained:

$$\Delta f_r|_{EI} = 100\left[\left(\frac{EI_{D3}}{EI}\right)^{0.5} - 1\right]$$

where: EI and EI_{D3} = the stiffness of the undamaged RC beam and evaluated by means the experimental diagrams moment, M, vs curvature, χ (Fig. 31).

The comparison between the frequency variations obtained both with the experimental data from dynamic vibrational tests and from static tests by the stiffnesses' ratio is good for the model type B, with a difference about 10%, and for type C, with a difference of 4%. The difference is instead about 30% for model type A. However, it is important to underline that in the case of beam type A the damage is particularly sever because it is located at the mid span section with great influence on the response under bending moment for the bending tests.

6. Conclusions

This paper presents an experimental research carried out on four RC beams damaged by notches and strengthened with EB GFRP strip with different configuration that may give a reflection on the damage related to vibration response by variation of frequency values as well as the static response of strengthened beams. The main results are the following:

1. The strengthening by EB GFRP strips led to a recovery of resistance in all the models damaged with notches and strengthened although the local damage by notch causes a loss of stiffness in RC beams.
2. In the case of beam models with damage located in lateral side respect to mid span section there was an increase of strength;
3. In all beam models strengthened with EB GFRP specimens an increase of ductility is mainly observed;
4. The strengthening by the EB GFRP strips on the compressive side of RC beam highlighted debonding mechanism resulting from local instability of the strengthening's strip glued;
5. The vibration tests permit to detect the damage by reduction of frequency values in presence of damage due to different width of notches;
6. The analysis of free vibration of the beams damaged by cracking of the concrete and strengthened using GFRP strip highlights that strengthening limits the damage state under bending conditions by reducing the width of the cracks undergoing even heavy loads, in this way limited frequency variations even for high bending moment values are shown;
7. Damage due to local buckling of the FRP layer on the compressed zone affects the response of strengthened RC beam and extensive investigation with theoretical analysis [36-38] have to be developed to know the mechanism of adhesion of GFRP strip under compressive stress.

Acknowledgement

This experimental research was supported by research funds provided by Università Politecnica delle Marche. The authors would like to express their gratitude to all the technicians and students who collaborated to develop the experimental research.

NOTATION

E_c = Young's modulus of concrete
f_y = yield strength of steel reinforcements
l = length of beam
h = height of beam
A = cross section area of beam
ρ = density
EI = bending stiffness of RC beam
$EI_{strength.}$ = bending stiffness of GFRP strengthened beam
I = moment of inertia of beam
ω = circular frequency value; angle of phase
λ = eigenvalue
Di = damage degree by notch
f, Δf = frequency value; difference between undamaged and damaged frequencies
$_r$ = index of vibration mode
E_{res} = Young's modulus of epoxy resin
ν_{res} = Poisson's coefficient of epoxy resin
t_{GFRP} = thickness of GFRP strip
f_{GFRP} = tensile strength of GFRP strip
E_{GFRP} = Young's modulus of GFRP strip
P = load
D*i = damage degree for cracking of concrete
$_{intr., ext.}$ = index for intrados and extrados of beam
ε_c = strain of compressive concrete
ε_{ct} = strain of tensile concrete
ε_{GFRP} = GFRP strain
M = bending moment
χ = curvature

References

1. Meier U. Bridge repair with high performance composite materials. Material und Technick 1987; **4**:125-128.
2. MPA. Bonding of Steel and GFRP Plates in the area of Coupling Joints. Talbrucke Hattenbusch. Federal Institute for Materials Testing, Braunschweg, Res. Report Nº3126/1429, 1987.
3. Saadatmanesh H., Ehsani M.R. RC beams strengthened with GFRP plates. I: experimental study. Journal of structural engineering 1991; **117**(11): 3417-3433.
4. An W., Saadatmanesh H., Ehsani M.R. RC beams strengthened with FRP plates. II: analysis and parametric study. J. of Structural Eng. 1991; **117**(11): 3434-3455.
5. Plevris N., Triantafillou T.C. Strengthening of RC beams with epoxy-bonded fibre composite materials. Materials and Structures 1992; **25**: 201-211.
6. Michaluk C.R., Rizkalla S.H., Tadros G., Benmokrane B. Flexural behaviour of one-way concrete slabs reinforced by fibre reinforced plastic reinforcements. ACI Structural Journal 1998; **95**(3): 353-365.
7. Ross C.A., Jerome D.M., Tedesco J.W., Huges M.L. Strengthening of reinforced concrete beams with externally bonded composite laminates. ACI Structural Journal 1999; **96**(2): 212-220.
8. Capozucca R., Ricci V. Bond of GFRP strips on modern and historic brickwork masonry. Composite Structures 2016; **140**: 540-555.
9. De Lorenzis L., Teng J.G. Near-Surface mounted FRP reinforcement: an emerging technique for strengthening structures. Composites Part B: Eng. 2007; **38**: 119-143.
10. Capozucca R. Static and dynamic response of damaged RC beams strengthened with NSM CFRP rods. Composite Structures 2009; **91**: 237-248.
11. Sena Cruz J.M., Barros J.A. O., Gettu R., Azevedo A.F.M. Bond behavior of near-surface mounted CFRP laminate strips under monotonic and cyclic loading. ASCE, Journal of Composites for Construction 2006; **10**: 295-303.
12. Sharaky I.A., Torres L., Baena M., Miàs C. An experimental study of different factors affecting the bond of NSM FRP bars in concrete. Composite Structures 2013; **99**: 350-365.
13. Capozucca R., Cerri M.N. Static and dynamic behaviour of RC beam model strengthened by CFRP-sheets. Constr. and Building Materials 2002; **16**: 91-99
14. Malek A.M., Saadatmanesh H. Analytical study of reinforced concrete beams strengthened with web-bonded fibre reinforced plastic plates or fabric. ACI Structural Journal 1998; **95**(3): 343-352.
15. Malek A.M., Saadatmanesh H., Ehsani M.R. Prediction of failure load of RC beams strengthened with FRP plate due to stress concentration at the plate end. ACI Structural Journal 1998; **95**(1): 142-152.
16. Arduini M, Di Tommaso A., Nanni A. Brittle failure in FRP plate and sheet bonded beams ACI Structural Journal 1997; **94**(4): 363-370.
17. Capozucca R. Analysis of bond-slip effects in RC beams strengthened with NSM CFRP rods. Composite Structures 2013; **102**: 110-123.
18. Capozucca R. On the strengthening of RC beams with near surface mounted GFRP rods. Composite Structures 2014, **117C**: 143-155.

19. Masmoudi A., Ouezdou M. Ben, Bouaziz J. New parameter design of GFRP RC beams. Construction and Building Materials 2012, **29**: 627-632.
20. Mansouri L., Djebbar A., Khatir S., Ali H.T., Behtani A., Wahab M.A. Static and fatigue behaviors of short glass fiber–reinforced polypropylene composites aged in a wet environment. Journal of Composite Materials 2019, **53**(23): 3629-3647.
21. Mansouri L., Djebbar A., Khatir S., Wahab M.A. Effect of hygrothermal aging in distilled and saline water on the mechanical behaviour of mixed short fibre/woven composites. Composite Structures 2019, **207**(1): 816-825.
22. Capozucca R. Vibration analysis of damaged RC beams strengthened with GFRP. Composite Structures 2018, **200**: 624-634.
23. Capozucca R. A reflection on the application of vibration tests for the assessment of cracking in PRC/RC beams. Engineering Structures 2013, **48**: 508-518.
24. Salawu O.S. Detection of structural damage through changes in frequency: a review. Engineering Structures 1997, 120: 2437-2450.
25. Khatir S., Brahim B., Capozucca R., Wahab M.A. Damage detection in CFRP composite beams based on vibration analysis using proper orthogonal decomposition method with radial basis functions and cuckoo search algorithm. Composite Structures 2018, **187**(1): 344-353.
26. Tiachacht S., Bouazzouni A., Khatir S., Wahab M.A., Behtani A., Capozucca R. Damage assessment in structures using combination of a modified Cornwell indicator and genetic algorithm. Engineering Structures 2018, **177**(15): 421-430.
27. Gillich G.R., Furdui H., Wahab M.A., Korka Z.I. A robust damage detection method based on multi-modal analysis in variable temperature conditions, Mechanical Systems and Signal Processing 2019, 115: 361–379.
28. Khatir S., Wahab M.A. Fast simulations for solving fracture mechanics inverse problems using POD-RBF XIGA and Jaya algorithmò Engineering Fracture Mechanics 2019, 205: 285–300.
29. Khatir S., Wahab M.A. A computational approach for crack identification in plate structures using XFEM, XIGA, PSO and Jaya algorithm. Theoretical and Applied Fracture Mechanics 2019, 103, 102240.
30. Khatir S., Wahab M.A., Boutchicha D., Khatir T. Structural health monitoring using modal strain energy damage indicator coupled with teaching-learning-based optimization algorithm and isogoemetric analysis, Sound and Vibration 2019, 448: 230-246.
31. Tran-Ngoc H., Khatir S., De Roeck G., Bui-Tien T., Nguyen-Ngoc L., Wahab M.A. Model Updating for Nam O Bridge Using Particle Swarm Optimization Algorithm and Genetic Algorithm. Sensors 2018, 18(12), 4131.
32. Warburton G.B. The dynamical behaviour of structures. Pergamon Press, 1964, Oxford.
33. EN 12390-3:2019. Testing hardened concrete - Part 3: Compressive strength of test specimens. European Standards, 2019.
34. EN ISO 15630-1:2019. Steel for the reinforcement and prestressing of concrete - Test methods - Part 1: Reinforcing bars, rods and wire. European Standards, 2019.
35. ASTM D 3039/D 3039 M - 08. Standard Test Method for Tensile Properties of Polymer Matrix Composite Materials. American Standard of Testing and Materials, 2008.
36. Kim Y., Davalos J.F., Barvero E.J. Delamination buckling of FRP layer in laminated wood beams. Compososite Strucures 1997, **37**(3–4): 311–320.

37. Bruno D. Delamination buckling in composite laminates with interlaminar defects. Theoretical and Applied Fracture Mechanics 1988, **9**(2): 145-159.

38. Kachanov L. Delamination buckling of composite materials. Springer Netherlands, 1988.

List of Figures:

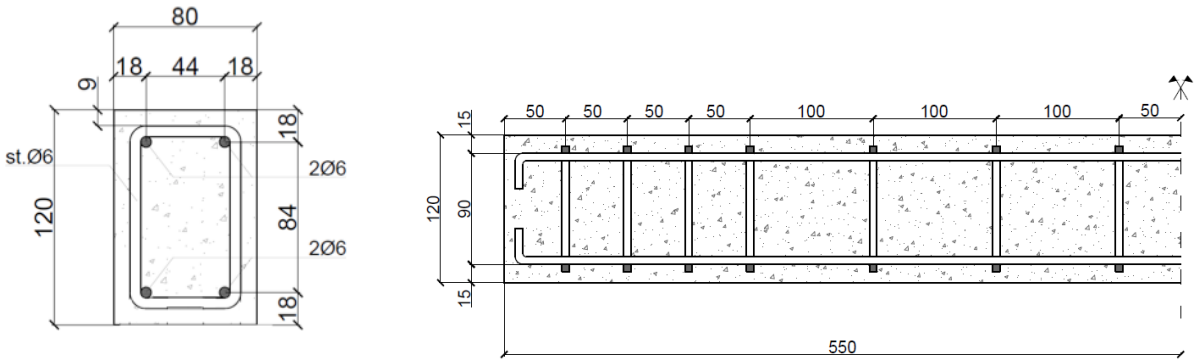

(a) (b)

Figure 1 – RC beam models: (a) cross section and (b) longitudinal section of RC beam with steel bars and stirrups.

(a)

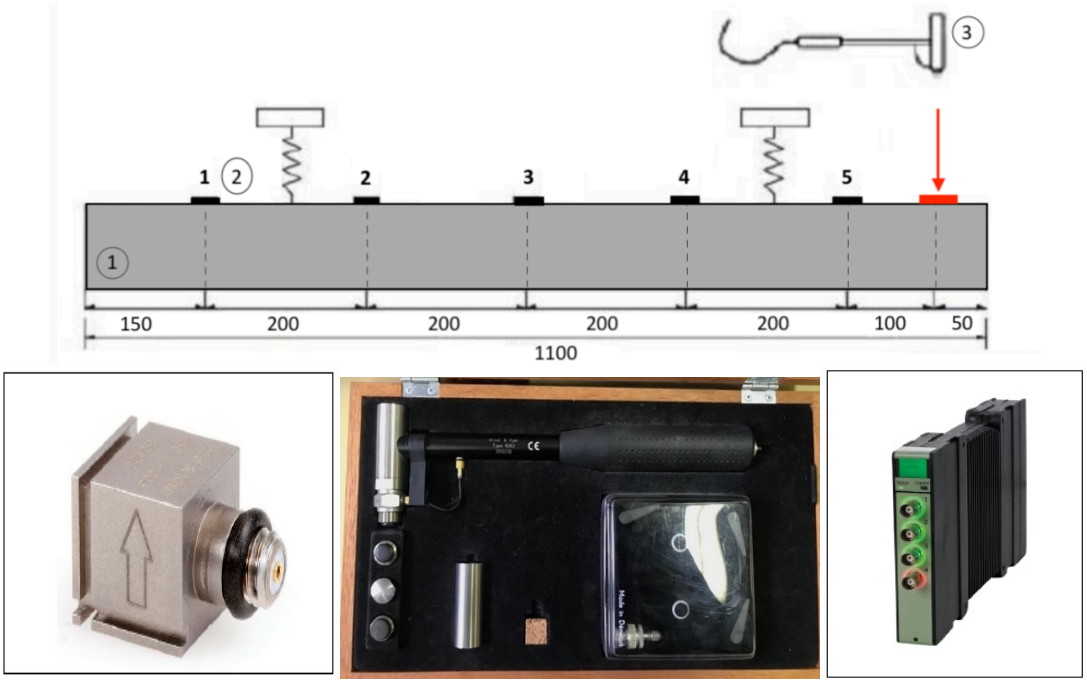

[2] [3] [4]

1. Beam 2. Accelerometer 3. Impact hammer 4. Analyzer FFT

(b)

Figure 2 – (a) RC beam hung to elastic springs and (b) set up for vibration tests.

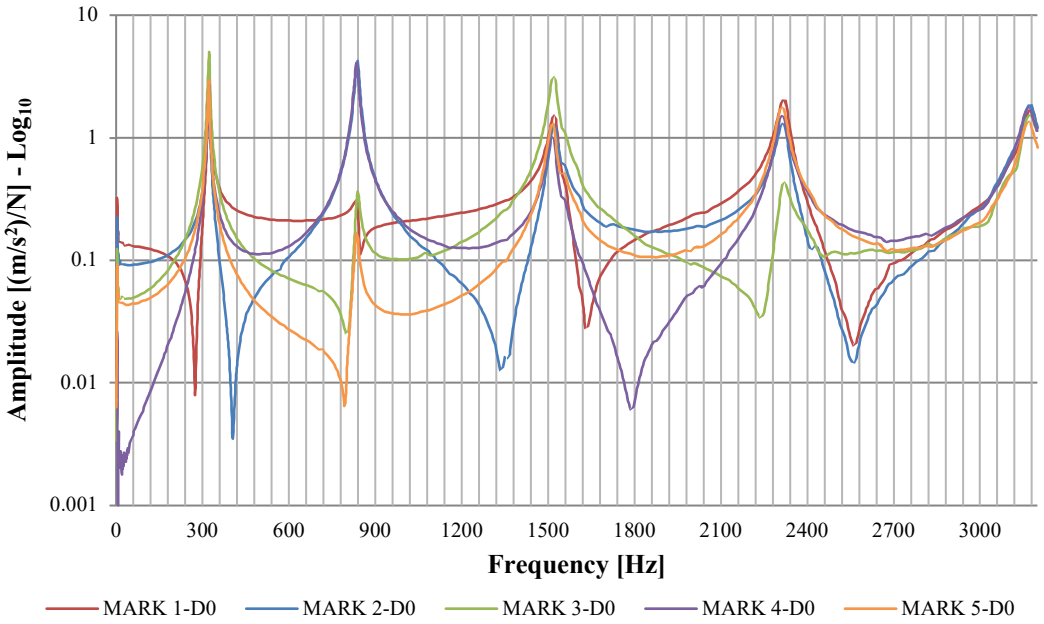

Figure 3 – Envelope of FRF by vibration tests on RC beam model (D0).

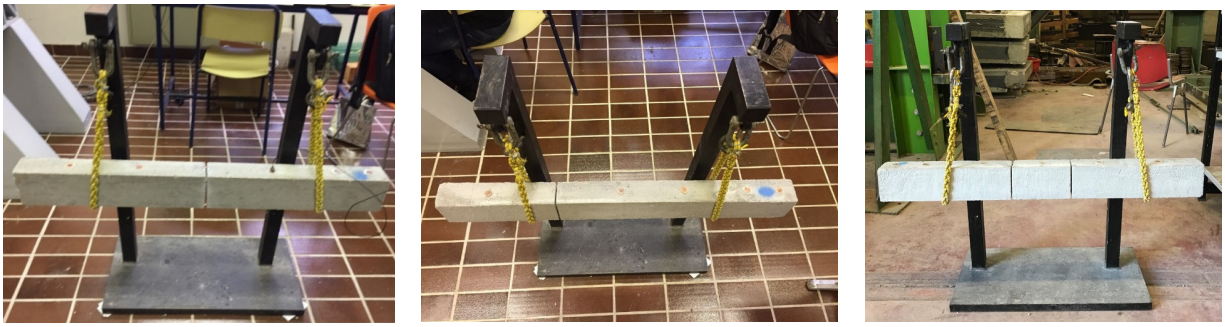

Damage type A | Damage – type B | Damage – type C

(a)

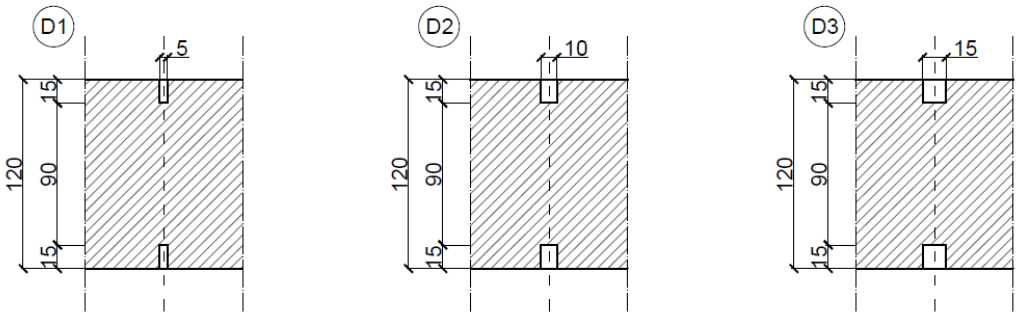

(b)

Figure 4 – (a) Damages in RC beam models: type A, B and C; (b) details of damage with different width of notch.

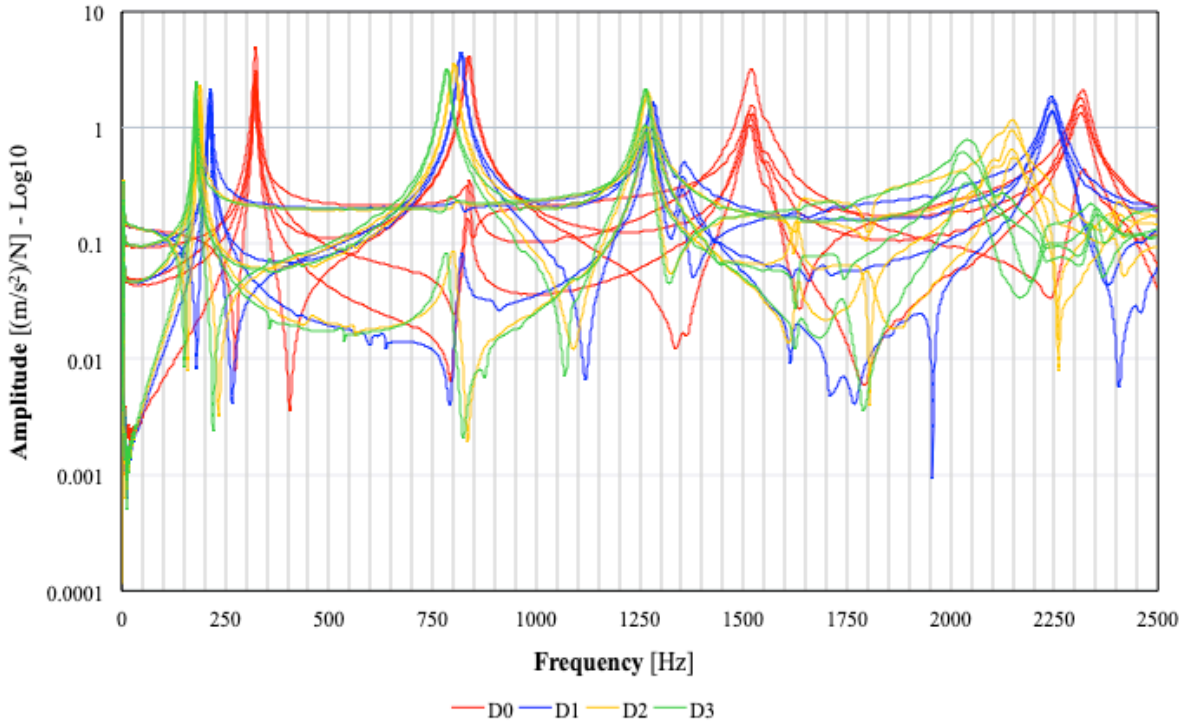

Figure 5 – Envelope diagrams of FRFs for damaged beam model type A at each damage degree D0, D1, …,D3 by notches.

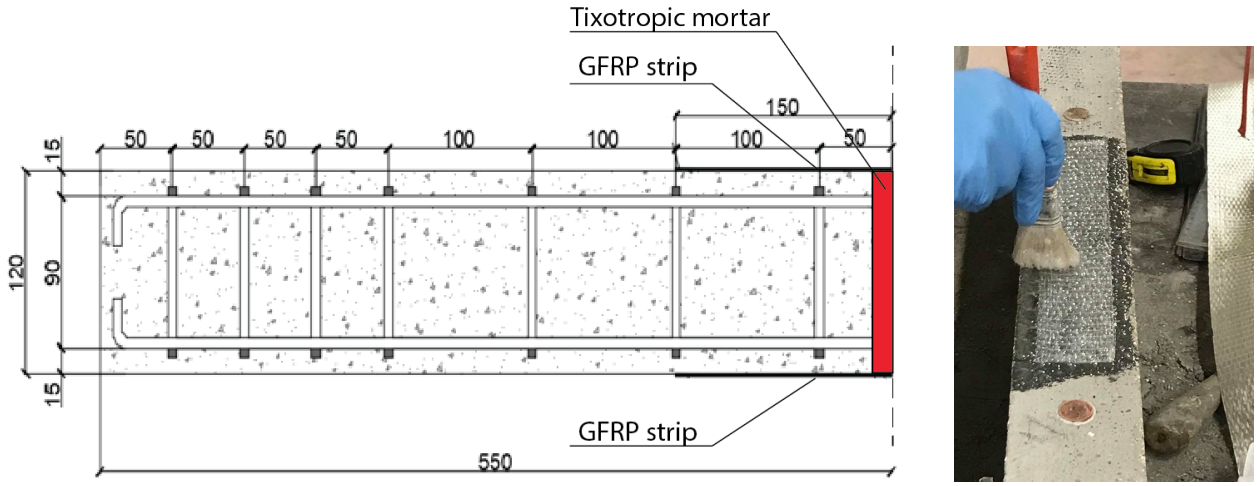

Figure 6 – RC beam with damage type A strengthened with thixotropic mortar and GFRP strips as R2 damage degree.

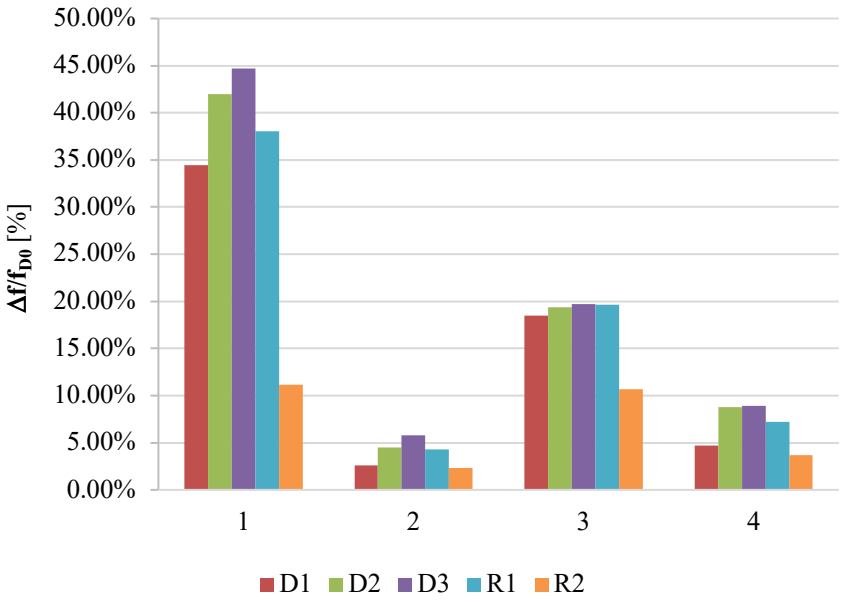

Figure 7 - Variation of exp. frequency values (%) at damage degree step for modes r = 1,...,4 in relation to D0 condition (beam damage type A).

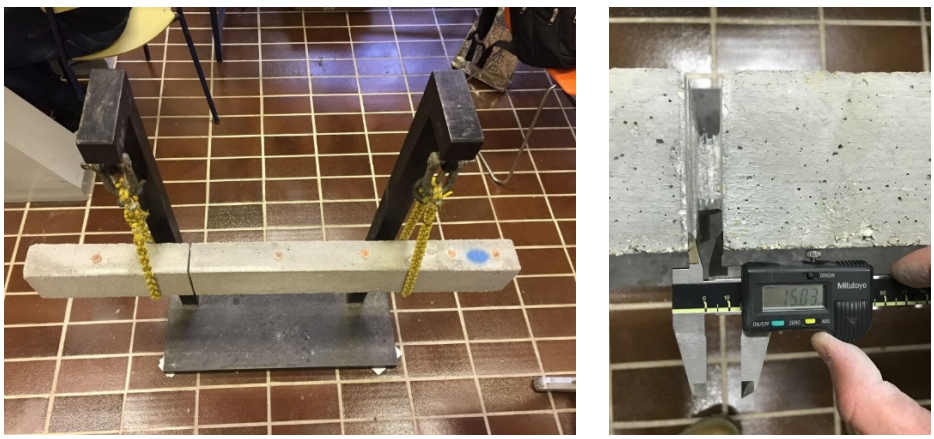

(a) (b)

Figure 8 - (a) Set up for vibration tests of beam model with damage type B due to lateral notch; (b) damage condition D3.

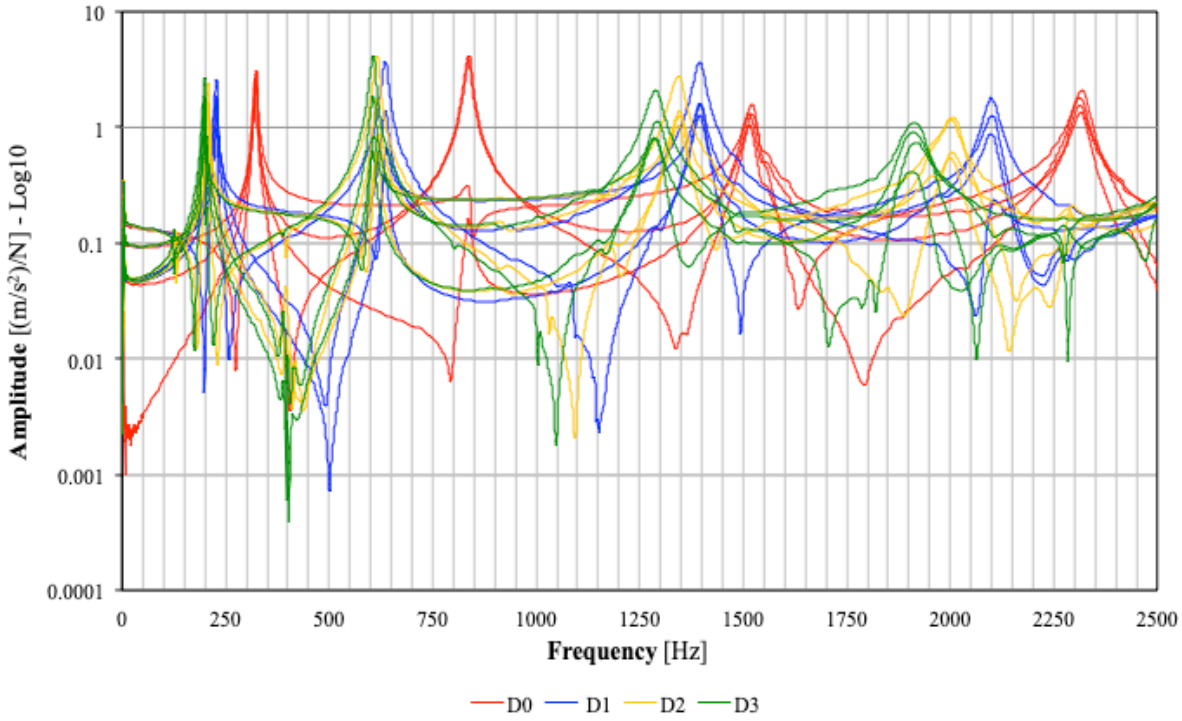

Figure 9 – Envelope diagrams of FRFs for damaged beam model type B at each damage degree D0, D1,…,D3 by notches.

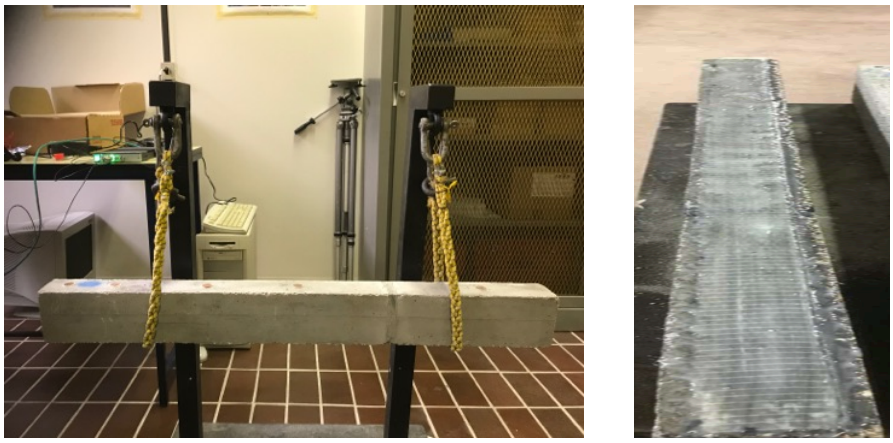

(a) (b)

Figure 10 – (a) Configuration R1 for beam type B where notch is filled with thixotropic mortar; (b) configuration R2 with GFRP strip at the intradoss.

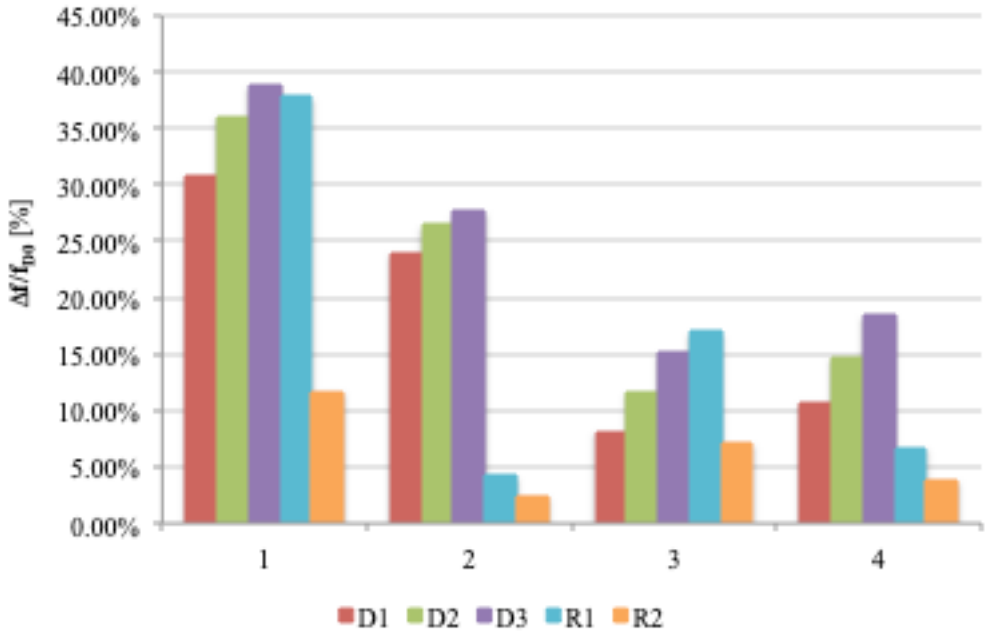

Figure 11 - Variation of exp. frequency values (%) at damage degree step for modes r = 1,...,4 in relation to D0 condition (beam with damage type B).

Figure 12 – Set up for vibration tests of beam type C with symmetric damage by notches.

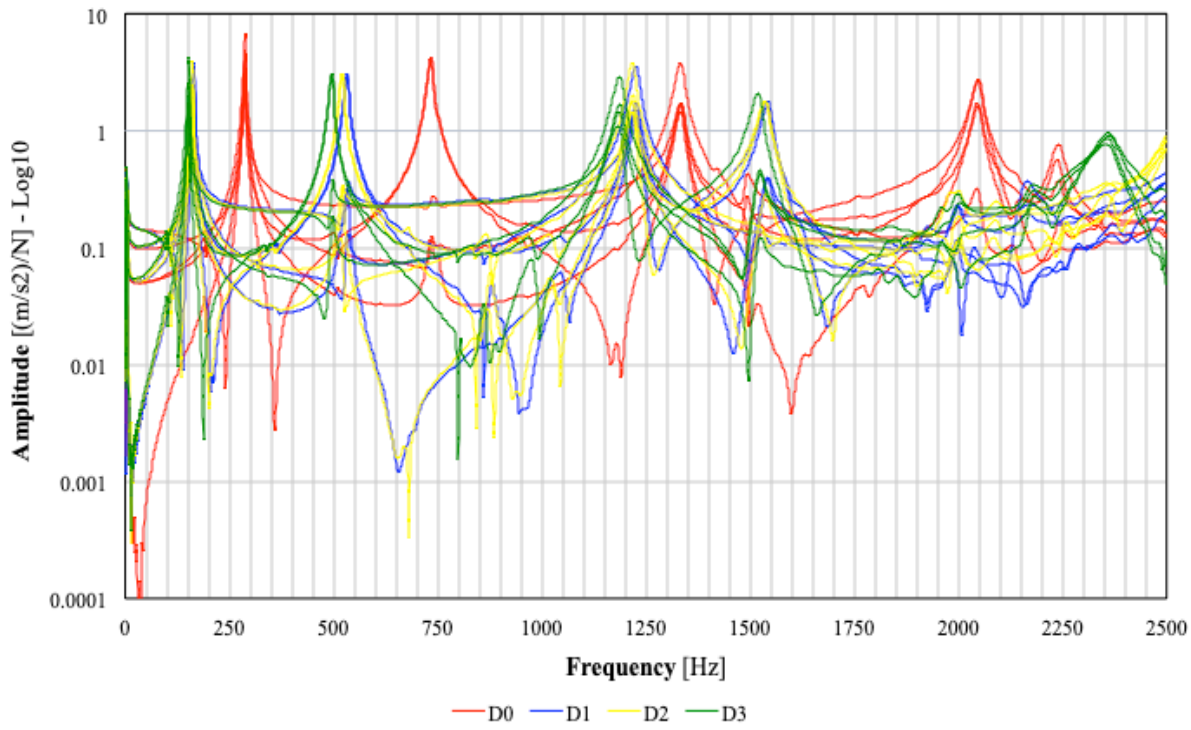

Figure 13 - Envelope of FRFs for damaged beam model type C at each damage degree by notches.

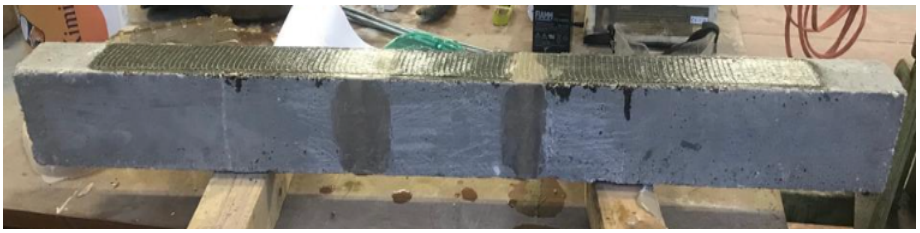

Figure 14 - Configuration R2 for beam type C: notches filled with thixotropic mortar and EB GFRP strip at intradoss.

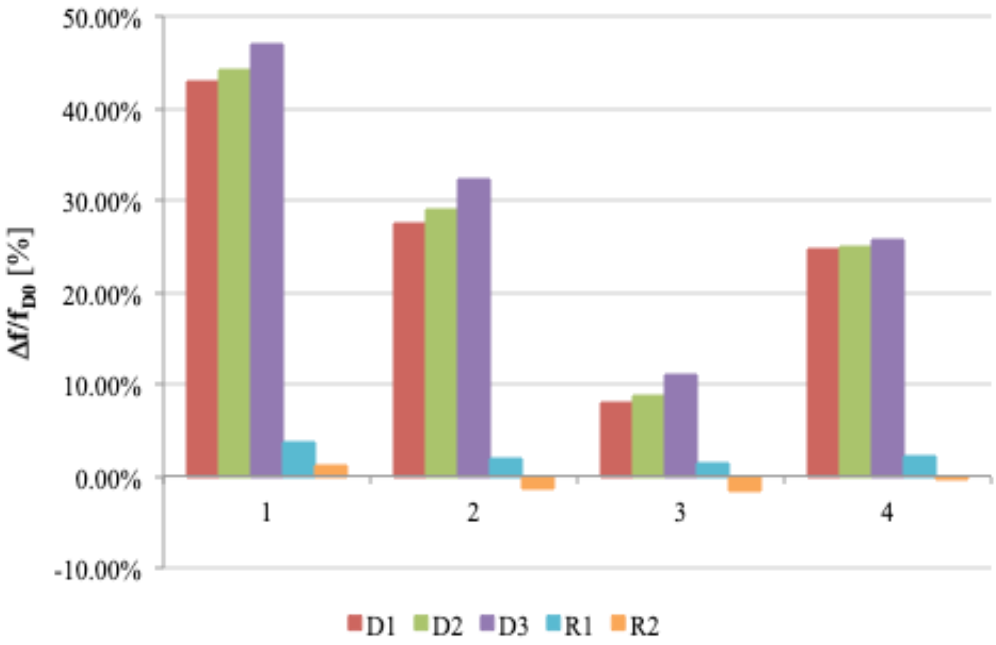

Figure 15 - Variation of exp. frequency values (%) at damage degree step for modes r = 1,...,4 in relation to D0 condition (beam type C).

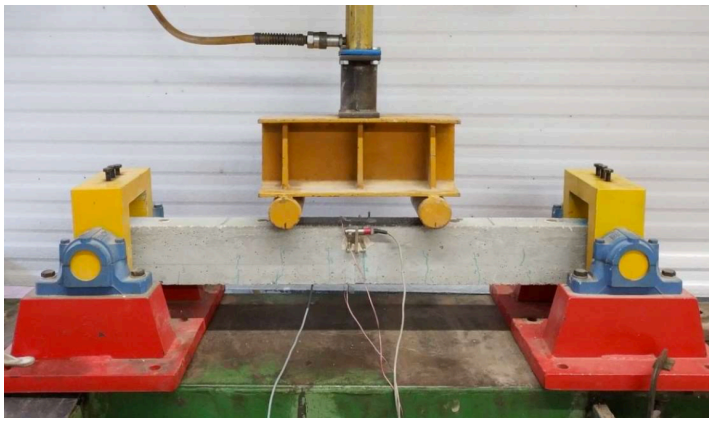

(a)

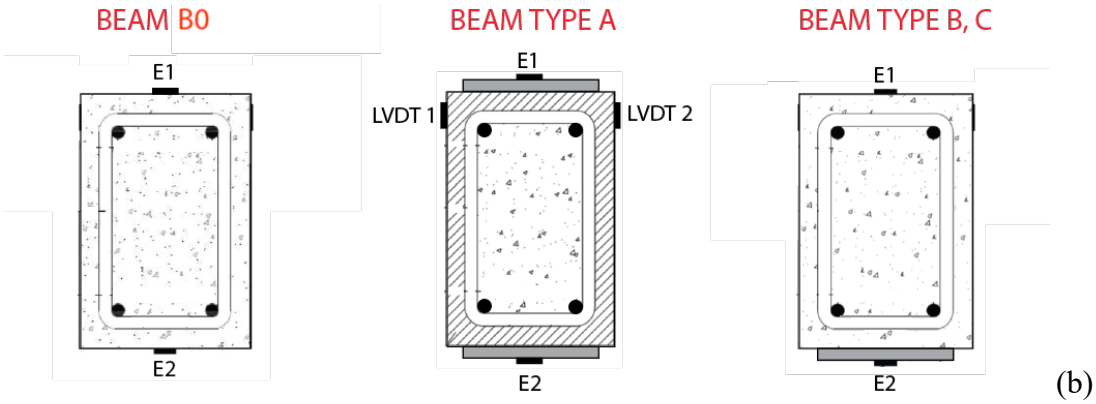

(b)

Figure 16 – (a) Set up of static bending tests; (b) location of instruments to measure strain at midspan section for tested beams.


(a)


(b)

Figure 17 – (a) View of beam B0 at failure; (b) detail of cracking with detachment of compressive concrete.

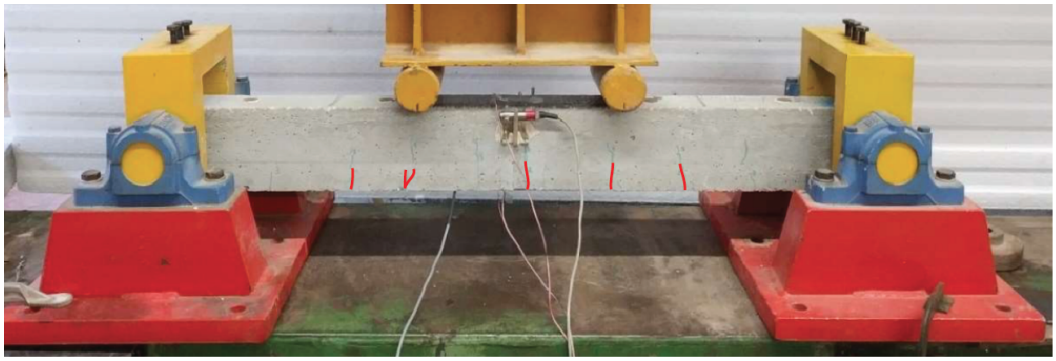

D*1

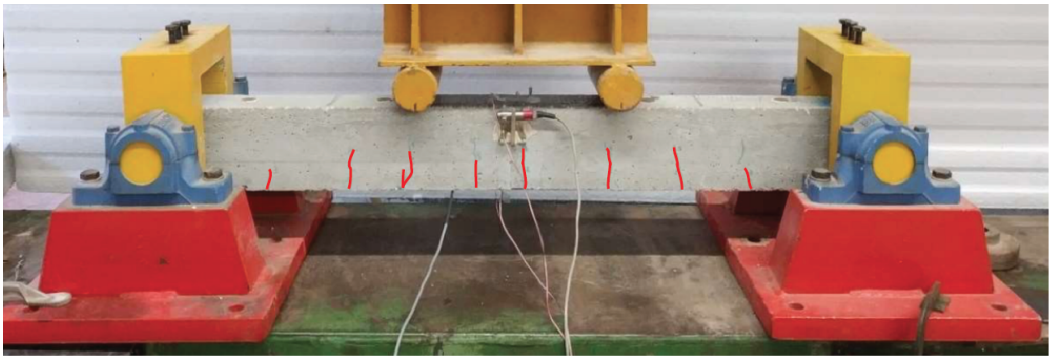

D*2

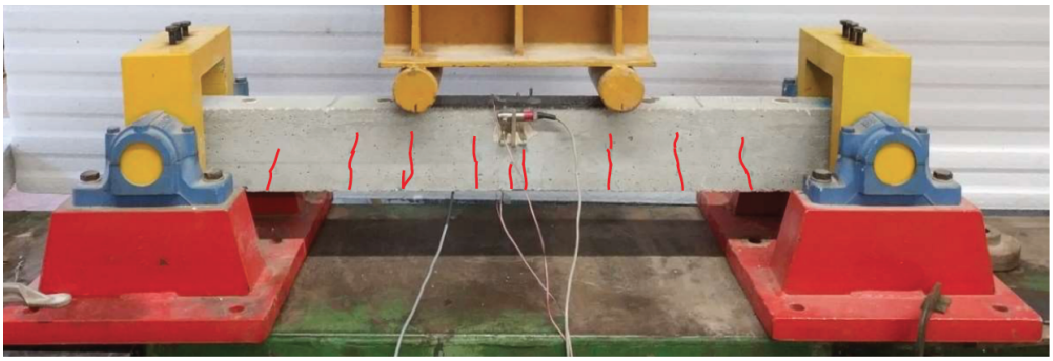

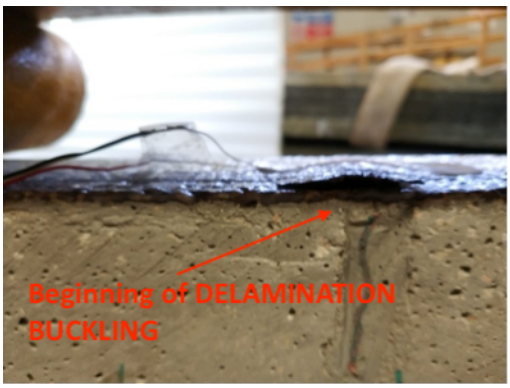

D*3

Figure 18 - Cracking damage development due to bending test for beam with damage type A and strengthening by GFRP strips.

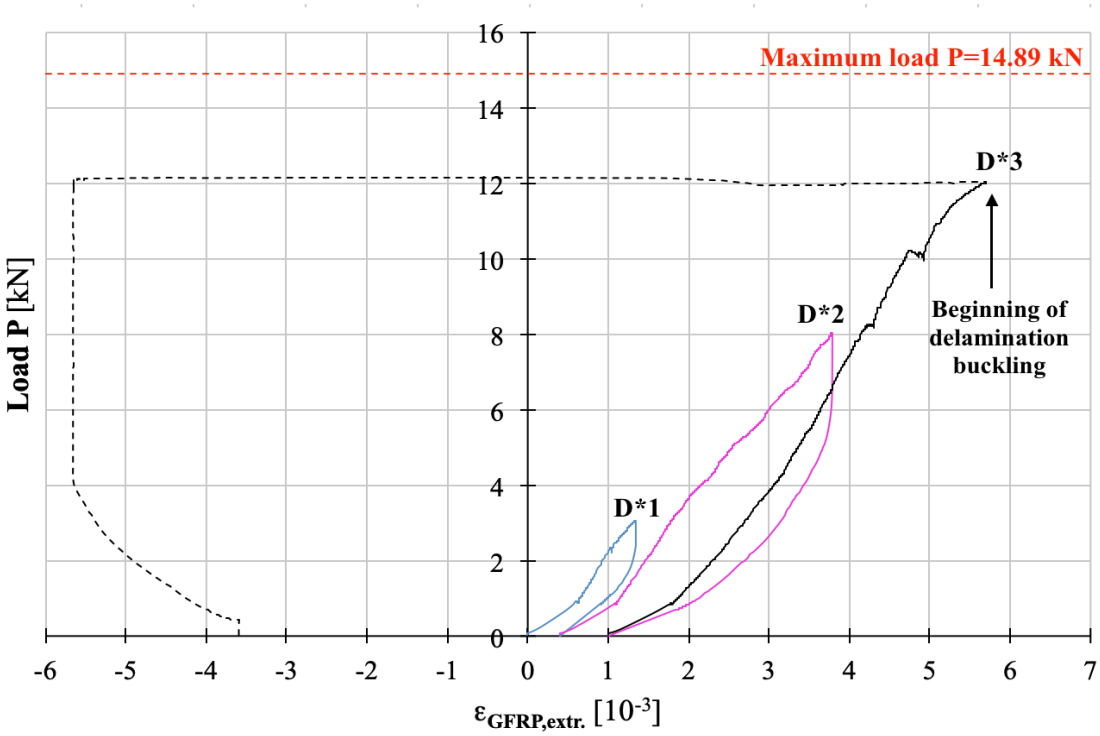

(a)

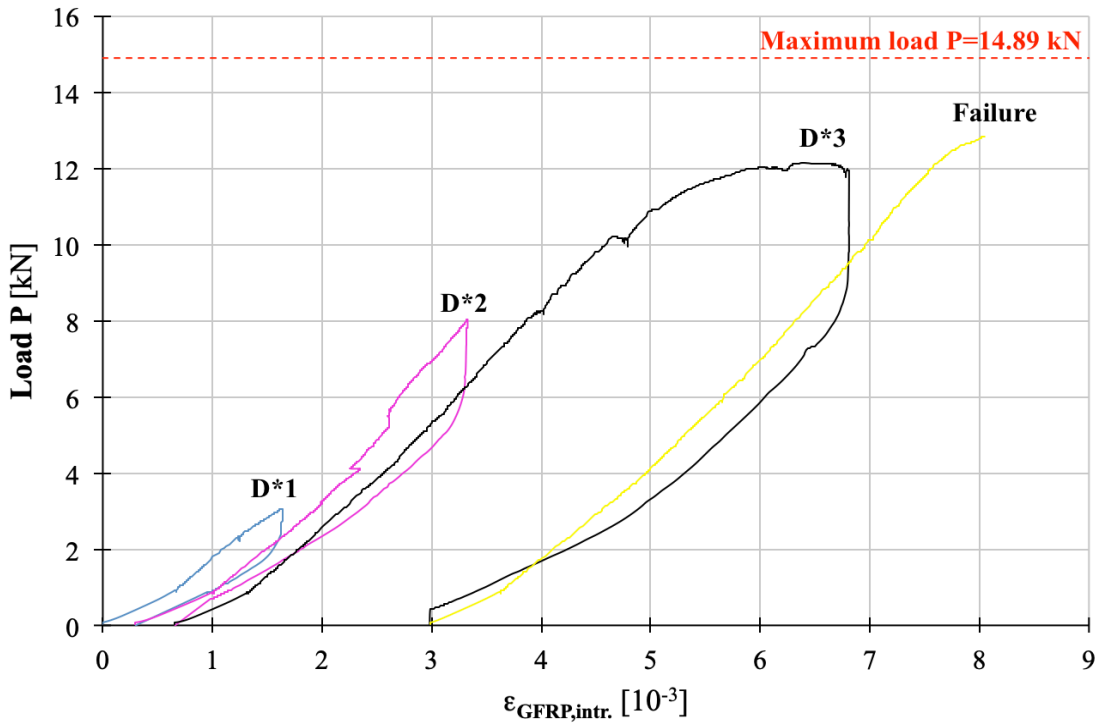

(b)

Figure 19 – (a) Exp. diagram load, P, vs strain of GFRP strip, $\varepsilon_{GFRP,extr.}$, at the extradoss of beam with damage type A; (b) exp. diagram load, P, vs strain of GFRP strip, $\varepsilon_{GFRP,intr.}$, at the intradoss of beam.

Figure 20 – View of failure of strengthened beam type B with detail of GFRP rupture.

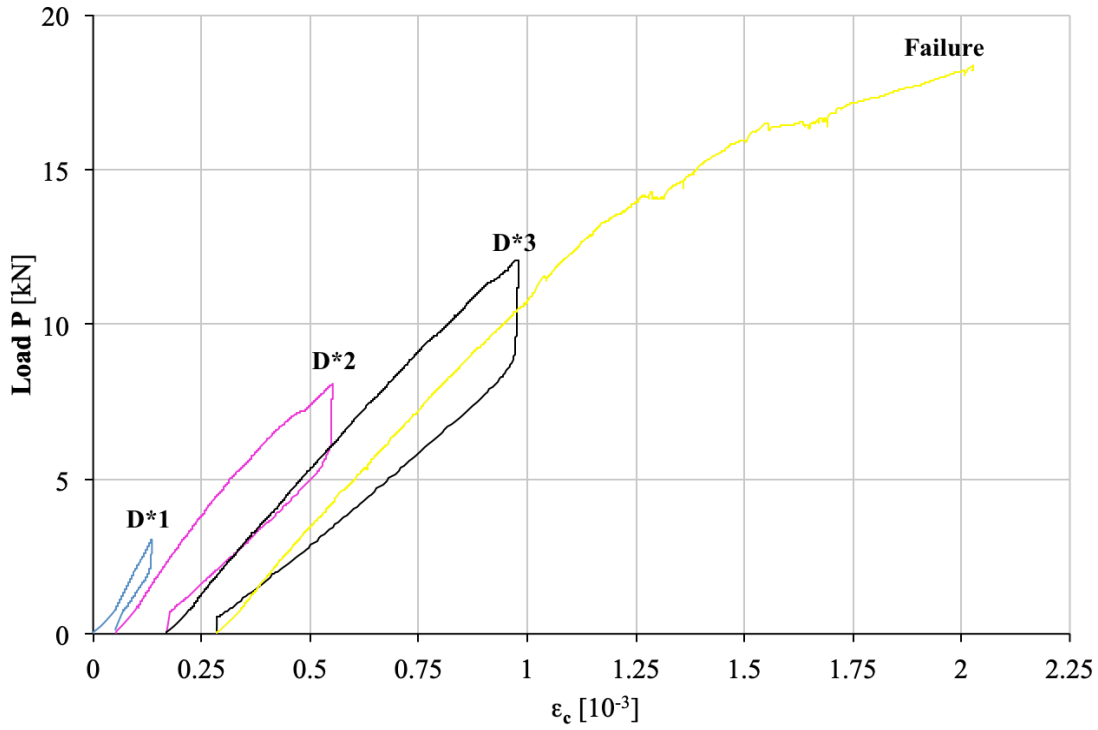

(a)

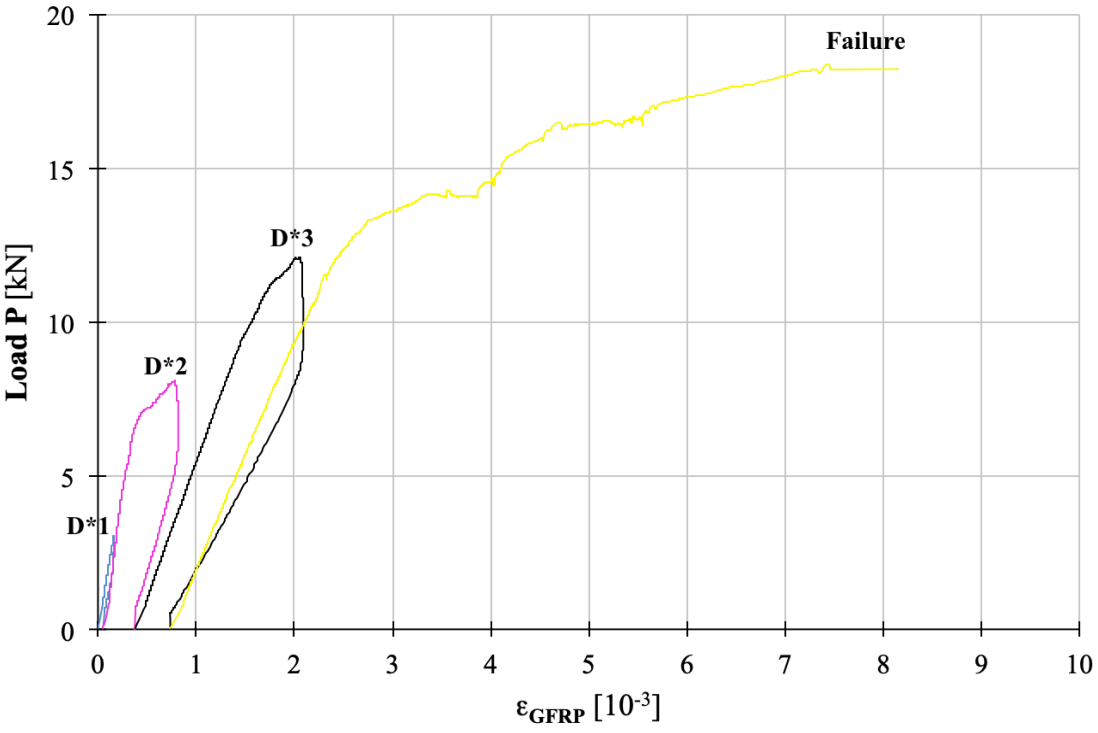

(b)

Figure 21 – (a) Exp. diagram load, P, vs strain of concrete, ε_c, at the edge of compressive concrete – beam with damage type B; (b) exp. diagram load, P, vs strain at the edge of tensile GFRP strip, ε_{GFRP}.

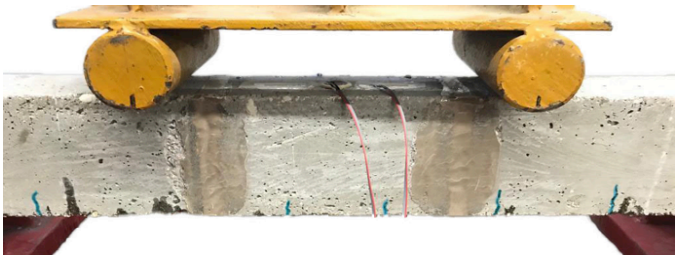

D*1

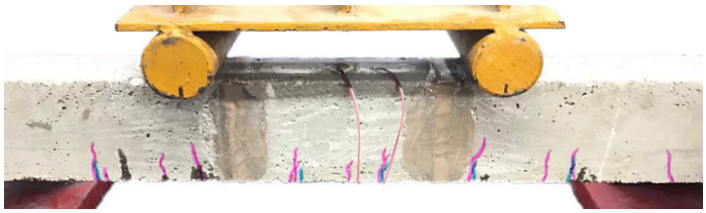

D*2

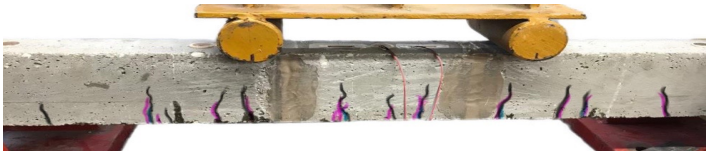

D*3

Failure

Figure 22 - Cracking damage development due to bending test at different damage degrees for strengthened beam with damage type C.

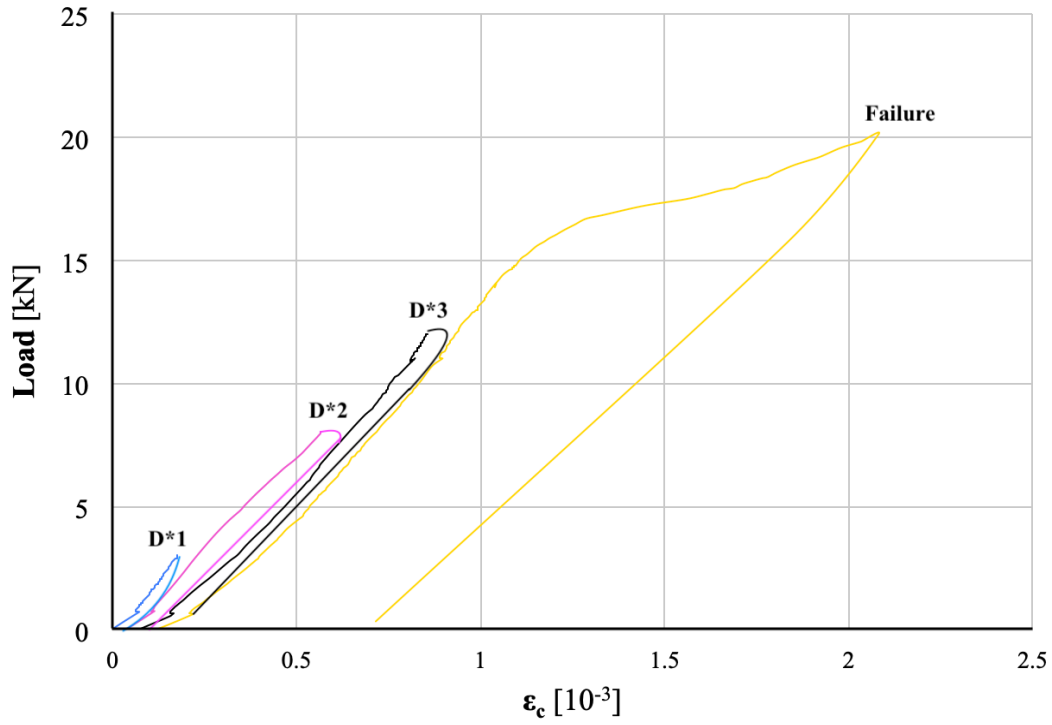

(a)

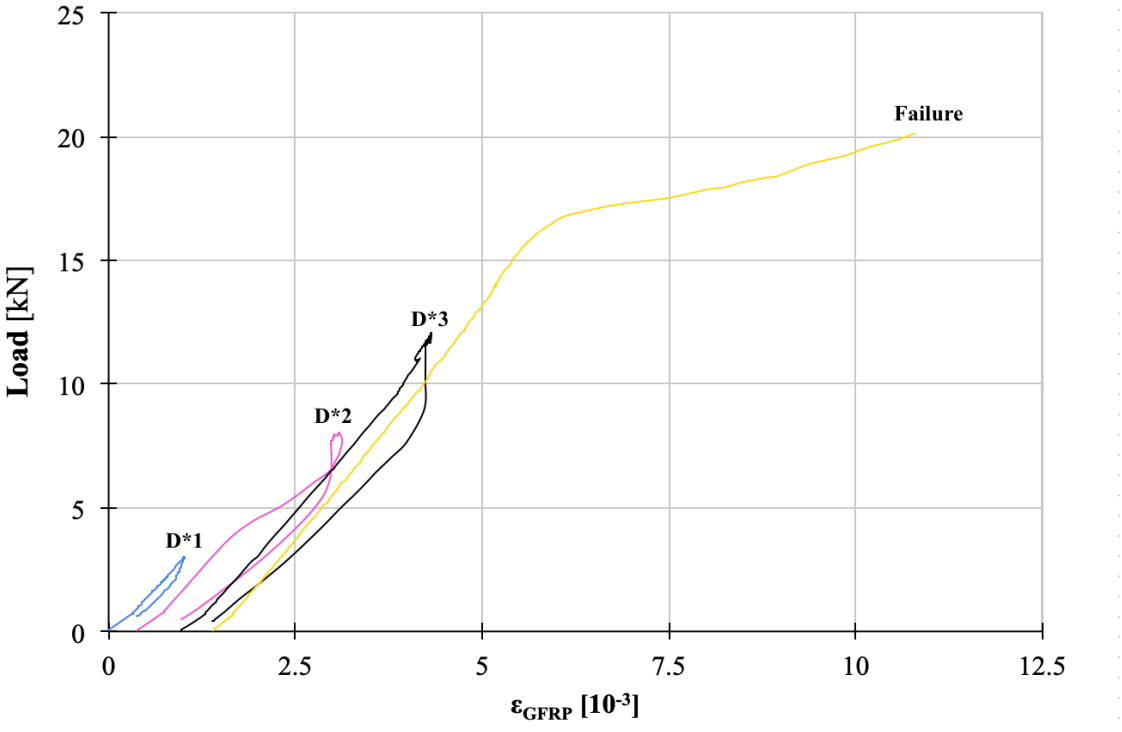

(b)

Figure 23 – (a) Exp. diagram load, P, vs strain of concrete, ε_c, at the edge of compressive concrete – beam with damage type C; (b) exp. diagram load, P, vs strain of GFRP strip, ε_{GFRP}.

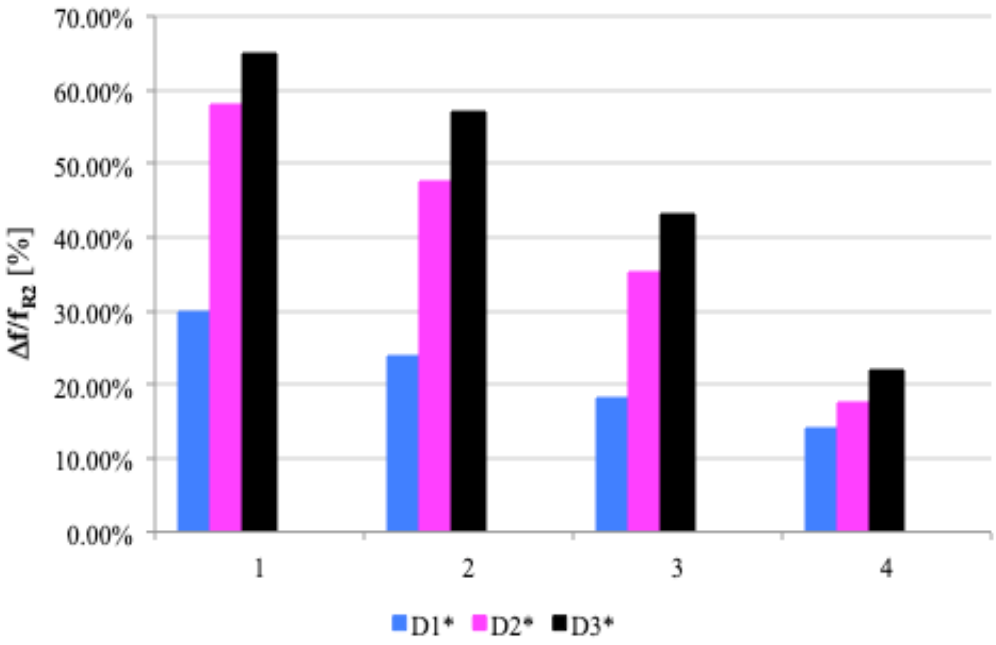

Figure 24 - Variation of exp. frequency values (%) at damage degree step by bending test for modes r = 1,...,4 in relation to D0 condition (beam B0).

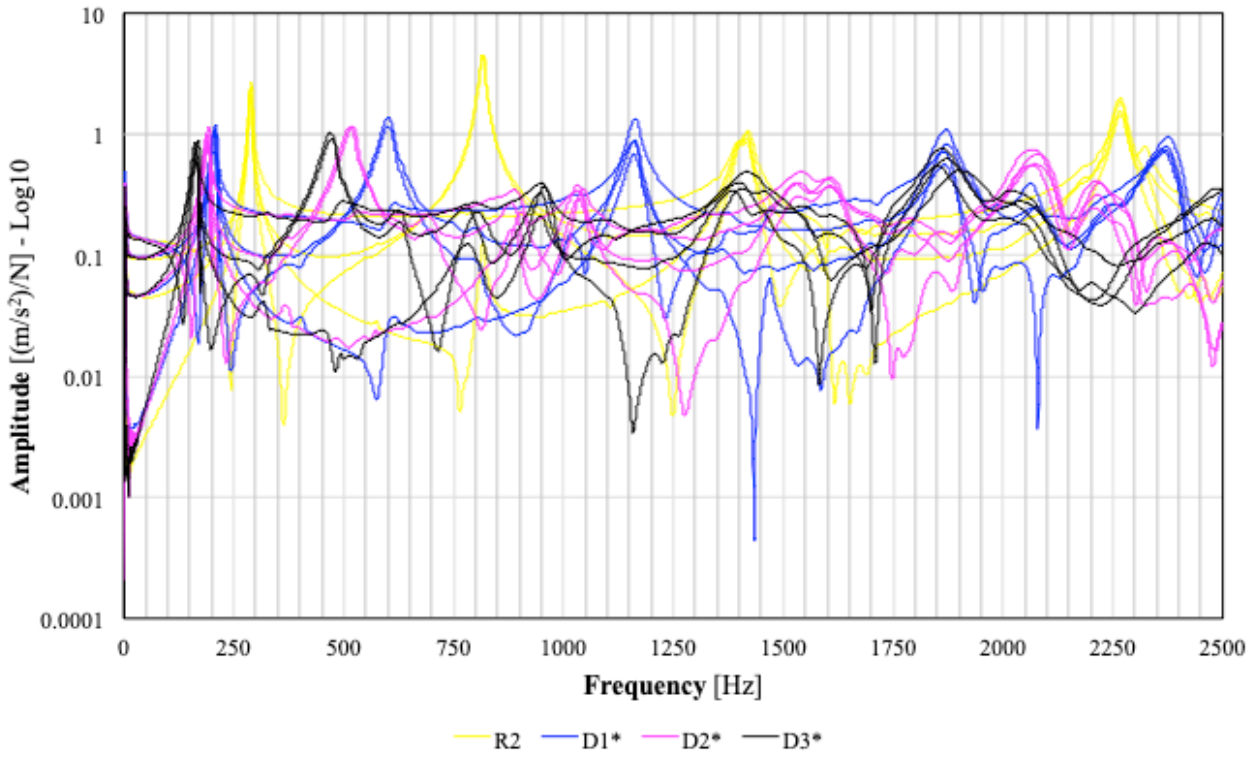

Figure 25 - Envelope of FRFs for damaged strengthened beam model type A at each damage degree by static bending test.

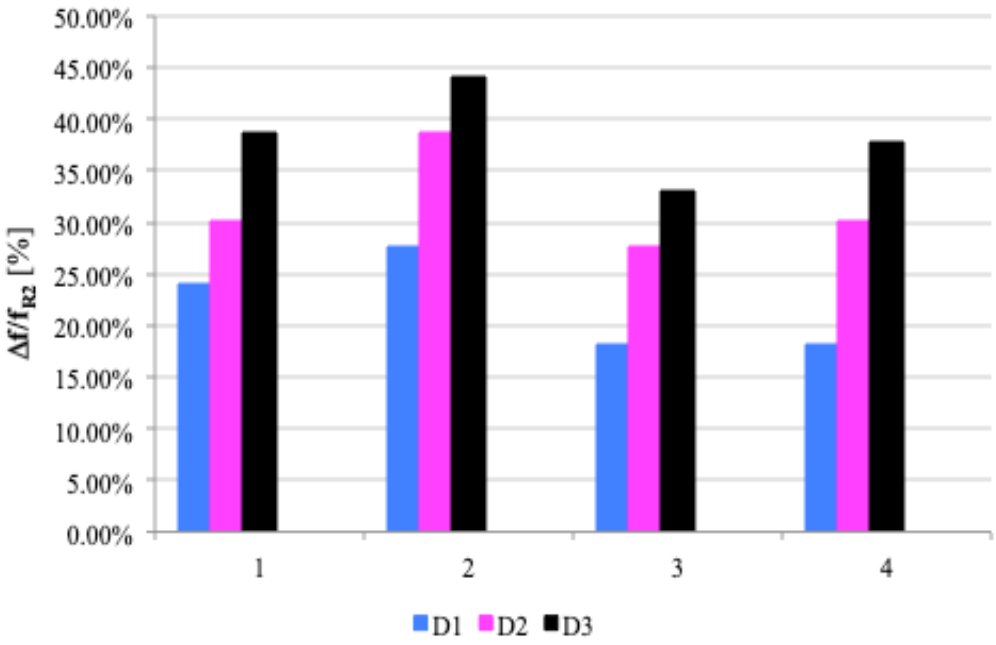

Figure 26 - Variation of exp. frequency values (%) at damage degree step by bending test for modes r = 1,...,4 in relation to R2 condition (beam type A).

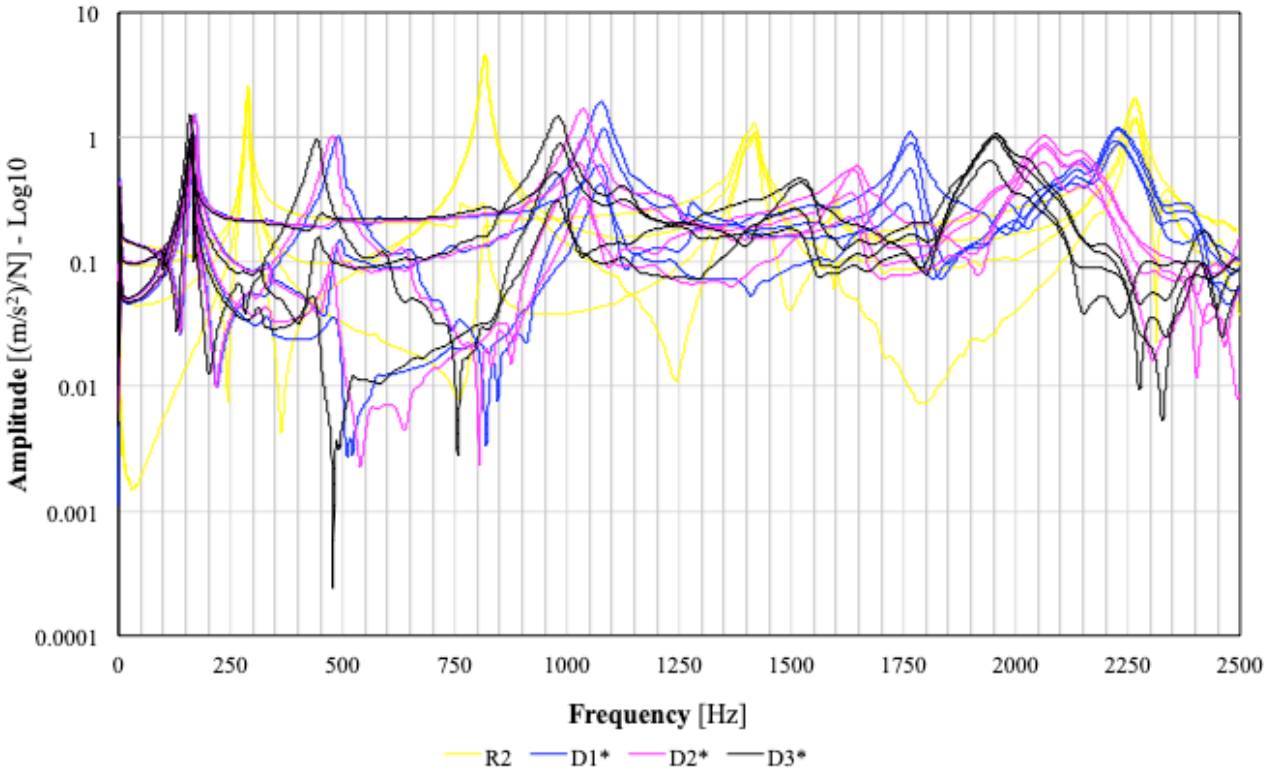

Figure 27 - Envelope of FRFs for damaged strengthened beam model type B at each damage degree by static bending test.

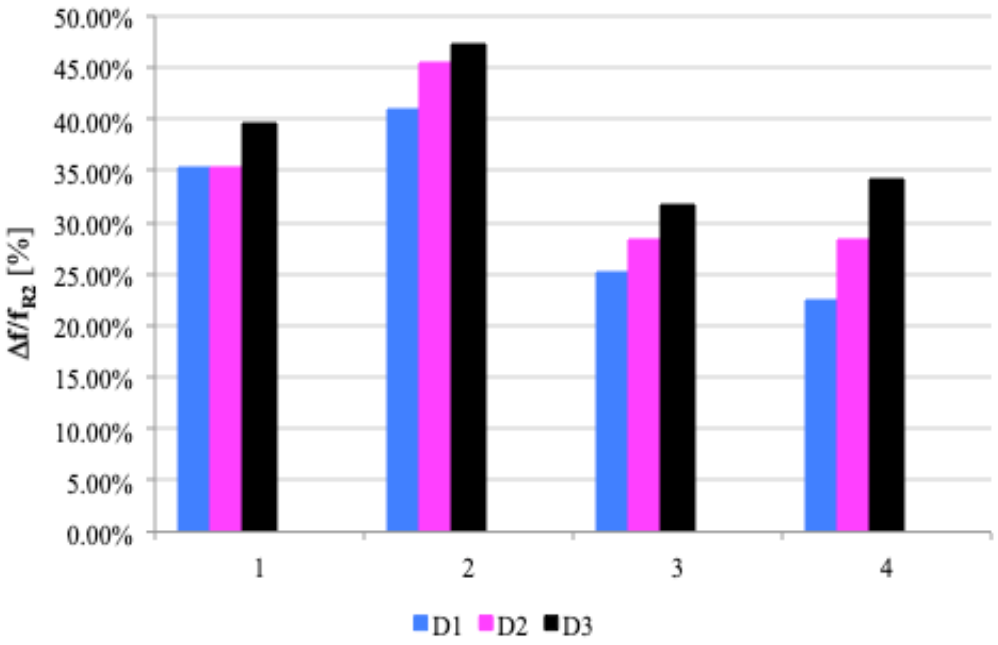

Figure 28 - Variation of exp. frequency values (%) at damage degree step by bending test for modes r = 1,...,4 in relation to R2 condition (beam type B).

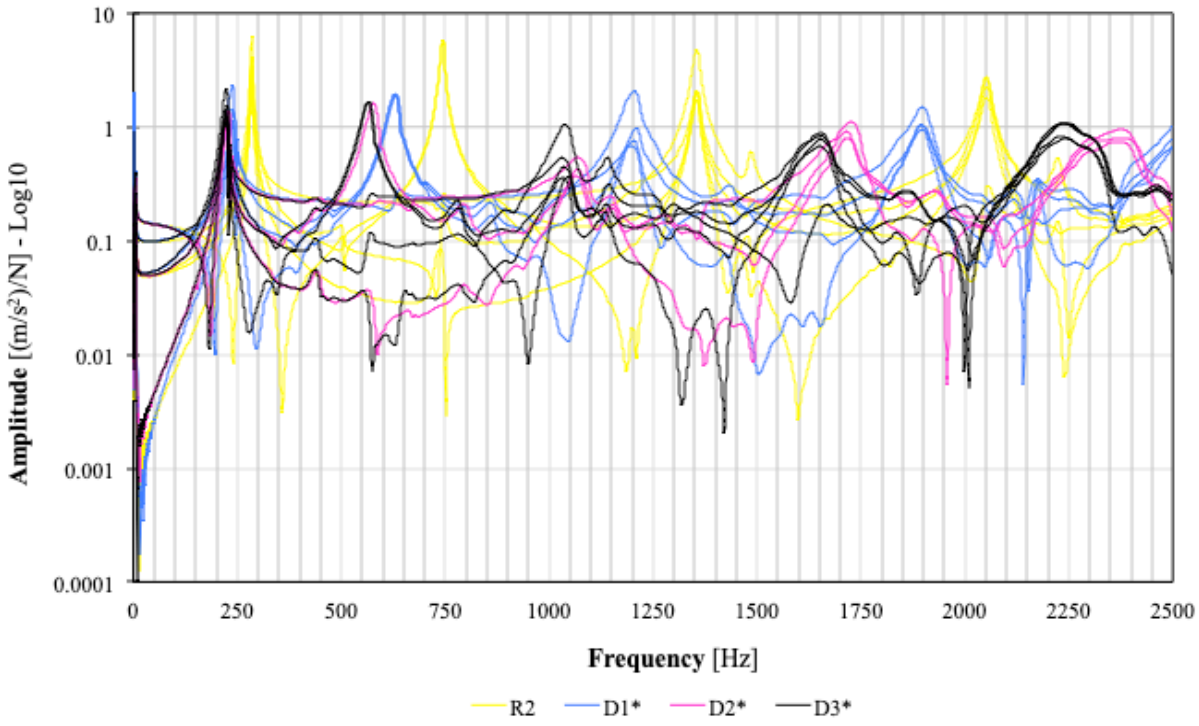

Figure 29 - Envelope of FRFs for damaged strengthened beam model type C at each damage degree by static bending test.

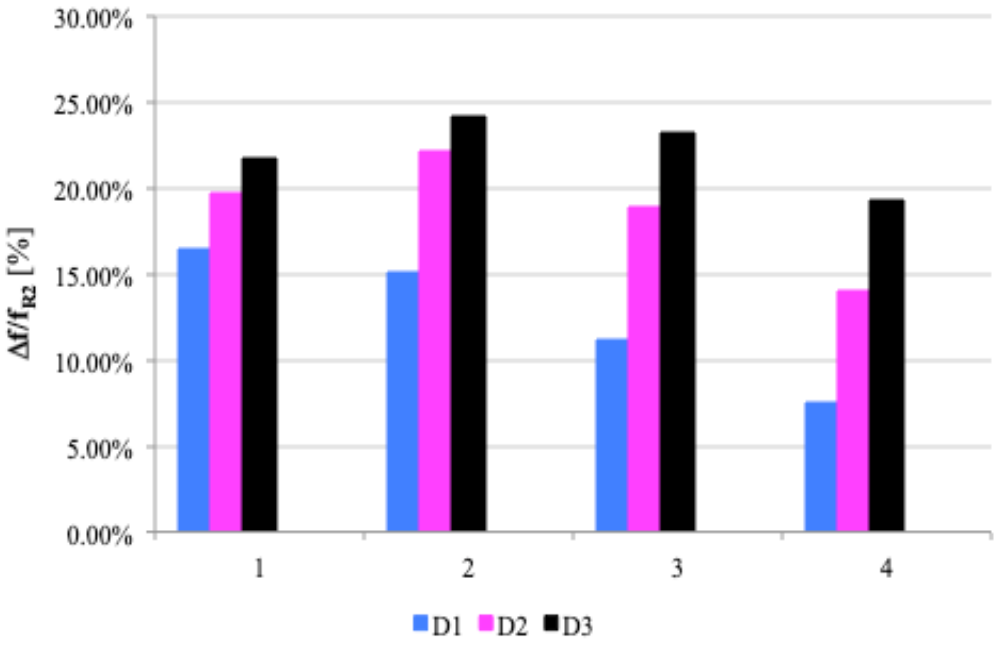

Figure 30 - Variation of exp. frequency values (%) at damage degree step by bending test for modes r = 1,...,4 in relation to R2 condition (beam type C).

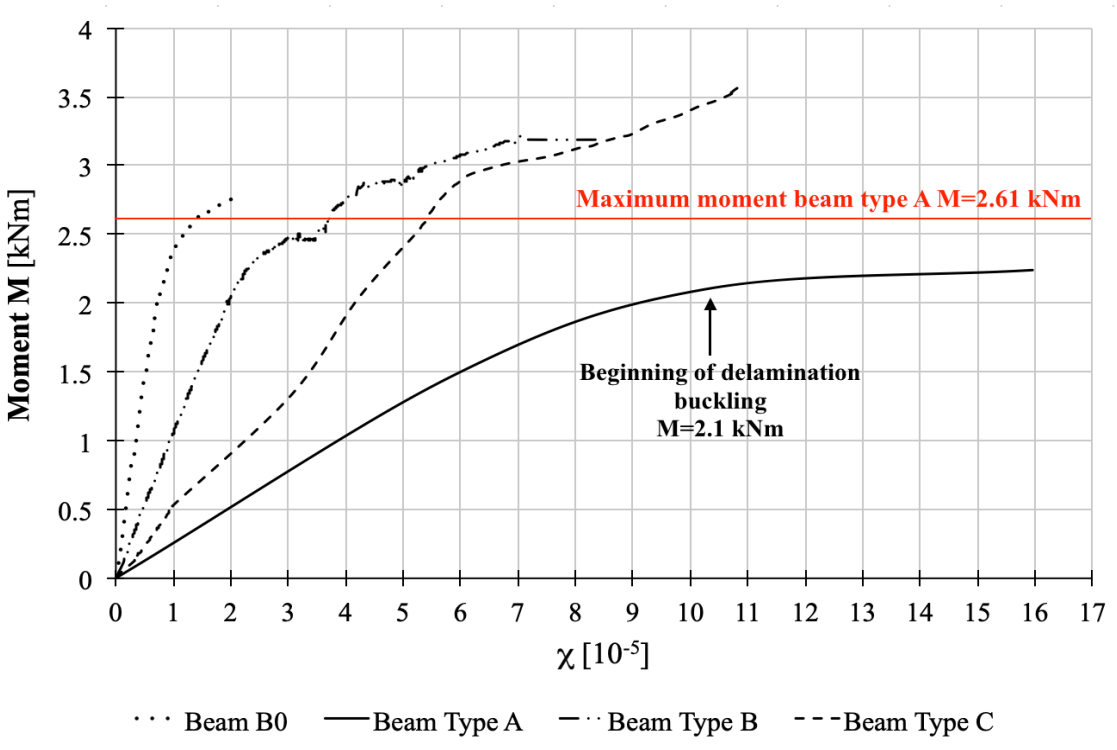

Figure 31 - Comparison between theoretical and experimental M vs. χ diagrams.

List of Tables:

Table 1 – Exp. data of RC beam models.

Width **b** [mm]	Height **h** [mm]	Length **L** [mm]	Young's modulus **E** [kN/mm^2]	Density **ρ** [Ns^2 /mm^4·10^{-9}]	Moment of inertia **I** [mm^4·10^3]
80	120	1100	28.43	2.370	11520

Table 2 - Theoretical and exp. frequency values of undamaged RC beam model.

Frequency values Undamaged RC Beam - D0	**f_1** [Hz]	**f_2** [Hz]	**f_3** [Hz]	**f_4** [Hz]
Euler-Bernoulli uniform beam	342	942	1847	3052
Experimental average values	323	835	1571	2352
FE numerical modeling	319.5	817.4	1532.3	2350.4

Table 3 – Exp. average frequency values at damage degree Di for RC beam model – Type A.

Damage Degree	**f_1** [Hz]	**$\Delta f_1/f_{D0}$** [%]	**f_2** [Hz]	**$\Delta f_2/f_{D0}$** [%]	**f_3** [Hz]	**$\Delta f_3/f_{D0}$** [%]	**f_4** [Hz]	**$\Delta f_4/f_{D0}$** [%]
D0	323	-	835	-	1571	-	2352	-
D1	211.72	34.45	813.08	2.63	1280.29	18.50	2241.86	4.68
D2	187.43	41.97	797.47	4.49	1266.66	19.37	2145.19	8.79
D3	178.54	44.72	786.59	5.80	1261.72	19.69	2141.76	8.94
R1	200.00	38.06	799.39	4.26	1262.16	19.66	2181.74	7.24
R2	287.05	11.13	815.38	2.35	1403.62	10.65	2264.88	3.70

Table 4 – Exp. average frequency values at damage degree D_i for RC beam model – Type B.

Damage Degree	**f_1** [Hz]	**$\Delta f_1/f_{D0}$** [%]	**f_2** [Hz]	**$\Delta f_2/f_{D0}$** [%]	**f_3** [Hz]	**$\Delta f_3/f_{D0}$** [%]	**f_4** [Hz]	**$\Delta f_4/f_{D0}$** [%]
D0	323.25	-	835.28	-	1517.79	-	2352.58	-
D1	223.64	30.82	635.01	23.98	1393.66	8.18	2098.81	10.79
D2	206.49	36.12	614.27	26.46	1341.3	11.63	2004.82	14.78
D3	197.78	38.82	604.28	27.66	1287.66	15.16	1922.13	18.42
R1	201.08	37.79	800.02	4.22	1260.5	16.95	2194.8	6.71
R2	285.30	11.74	815.16	2.41	1409.93	7.11	2262.67	3.82

Table 5 – Exp. average frequency values at damage degree D_i for RC beam model – Type C.

Damage Degree	**f_1** [Hz]	**$\Delta f_1/f_{D0}$** [%]	**f_2** [Hz]	**$\Delta f_2/f_{D0}$** [%]	**f_3** [Hz]	**$\Delta f_3/f_{D0}$** [%]	**f_4** [Hz]	**$\Delta f_4/f_{D0}$** [%]
D0	288.44	-	735.47	-	1333.75	-	2046.88	-
D1	164.85	42.85	534.22	27.36	1226.56	8.04	1542.19	24.66
D2	161.25	44.10	521.41	29.11	1217.97	8.68	1536.99	24.91
D3	153.13	46.91	497.65	32.34	1186.56	11.04	1522.81	25.60
R1	278.13	3.57	721.88	1.85	1314.22	1.46	2004.69	2.06
R2	285.16	1.14	745.05	-1.30	1355	-1.59	2053.28	-0.31

Table 6 – Exp. results for beam B0 under static bending test.

Damage steps	Load [kN]	Moment [kNm]	Strain at compressive concrete ε_c (‰)	Strain at tensile concrete ε_{ct} (‰)	Curvature of midspan section χ (10^{-5})
D*1	3.00	0.53	0.24	0.01	0.21
D*2	8.00	1.40	0.65	0.08	0.62
D*3	12.00	2.10	0.91	0.09	0.83
Failure	15.77	2.76	2.54	0.28	2.35

Table 7 – Exp. results for beam with damage type A and strengthening with GFRP strips under static bending test.

Damage steps	Load [kN]	Moment [kNm]	Strain at compressive concrete ε_c (‰)	Strain at GFRP strip (extrados) $\varepsilon_{GFRP,ext}$ (‰)	Strain at GFRP strip (intrados) $\varepsilon_{GFRP,int}$ (‰)	Curvature of midspan section χ (10^{-5})
D*1	4.00	0.53	-	1.19	1.51	2.25
D*2	8.00	1.40	-	3.78	3.32	5.92
D*3	12.00	2.10	-	5.69	6.62	10.25
Failure	14.89	2.61	3.87	-	-	-

Table 8 – Exp. results for beam with damage type B and strengthening with GFRP strip under static bending test.

Damage steps	Load [kN]	Moment [kNm]	Strain at compressive concrete ε_c (‰)	Strain at tensile GFRP strip ε_{GFRP} (‰)	Curvature of midspan section χ (10^{-5})
D*1	4.00	0.53	0.19	0.17	0.30
D*2	8.00	1.40	0.61	0.85	1.22
D*3	12.00	2.10	0.96	2.02	2.48
Failure	18.35	3.21	2.02	8.15	8.48

Table 9 – Exp. results for beam with damage type C and strengthening with GFRP strips under static bending test.

Damage steps	Load [kN]	Moment [kNm]	Strain at compressive concrete ε_c (‰)	Strain at tensile GFRP strip ε_{GFRP} (‰)	Curvature of midspan section χ (10^{-5})
D*1	4.00	0.53	0.16	0.91	0.89
D*2	8.00	1.40	0.56	3.12	3.07
D*3	12.00	2.10	0.84	4.23	4.22
Failure	20.35	3.53	2.08	10.85	10.78

Table 10 – Exp. average frequency values at damage degree Di for RC beam type B0.

Damage Degree	f_1 [Hz]	$\Delta f_1/f_{D0}$ [%]	f_2 [Hz]	$\Delta f_2/f_{D0}$ [%]	f_3 [Hz]	$\Delta f_3/f_{D0}$ [%]	f_4 [Hz]	$\Delta f_4/f_{D0}$ [%]
D0	288.28	-	734.38	-	1333.59	-	2046.88	-
D*1	202.34	29.81	560.16	23.72	1092.19	18.12	1756.25	14.20
D*2	121.09	58.00	385.15	47.55	864.84	35.15	1688.28	17.52
D*3	100.82	65.03	315.03	57.10	759.44	43.05	1595.40	22.06

Table 11 – Exp. average frequency values at damage degree Di for strengthened beam type A.

Damage Degree	f_1 [Hz]	$\Delta f_1/f_{D0}$ [%]	f_2 [Hz]	$\Delta f_2/f_{D0}$ [%]	f_3 [Hz]	$\Delta f_3/f_{D0}$ [%]	f_4 [Hz]	$\Delta f_4/f_{D0}$ [%]
R2	287.05	-	815.38	-	1403.62	-	2264.88	-
D*1	218.164	24.00	589.84	27.66	1150	18.07	1851.56 (*)	18.25
D*2	200.586	30.12	500	38.68	1016.40	27.59	1580.46 (*)	30.22
D*3	175.976	38.70	455.47	44.14	939.84	33.04	1410.16 (*)	37.74

(*) values of uncertain interpretation.

Table 12 – Exp. average frequency values at damage degree Di for strengthened beam type B.

Damage Degree	f_1 [Hz]	$\Delta f_1/f_{D0}$ [%]	f_2 [Hz]	$\Delta f_2/f_{D0}$ [%]	f_3 [Hz]	$\Delta f_3/f_{D0}$ [%]	f_4 [Hz]	$\Delta f_4/f_{D0}$ [%]
R2	285.30	-	815.16	-	1409.93	-	2262.67	-
D*1	184.77	35.24	481.25	40.96	1055.47	25.14	1755.47 (*)	22.42
D*2	184.77	35.24	443.75	45.56	1011.72	28.24	1621.88 (*)	28.32
D*3	172.07	39.69	429.69	47.29	962.5	31.73	1490.63 (*)	34.12

(*) values of uncertain interpretation.

Table 13 – Exp. average frequency values at damage degree Di for strengthened beam type C.

Damage Degree	f_1 [Hz]	$\Delta f_1/f_{D0}$ [%]	f_2 [Hz]	$\Delta f_2/f_{D0}$ [%]	f_3 [Hz]	$\Delta f_3/f_{D0}$ [%]	f_4 [Hz]	$\Delta f_4/f_{D0}$ [%]
R2	285.16	-	745.05	-	1355	-	2053.28	-
D*1	238.28	16.44	632.55	15.10	1204.38	11.12	1897.81	7.57
D*2	228.91	19.73	580.08	22.14	1099.06	18.89	1765.04	14.04
D*3	223.28	21.70	565.23	24.14	1040.23	23.23	1656.25	19.34